TU Delft

Delft University of Technology

Document Version
Final published version

Licence
CC BY-NC-ND

Citation (APA)
Castrillón-Franco, C., Rueda-Torres, J. L., & Román-Messina, A. (2026). Sub-Synchronous Oscillation Identification in Multi-Converter Energy Systems: Review and Assessment of Existing Signal Record-Based Methods. *IET Renewable Power Generation*, *20*(1), Article e70375. https://doi.org/10.1049/rpg2.70375

Important note
To cite this publication, please use the final published version (if applicable).
Please check the document version above.

Copyright
In case the licence states “Dutch Copyright Act (Article 25fa)”, this publication was made available Green Open Access via the TU Delft Institutional Repository pursuant to Dutch Copyright Act (Article 25fa, the Taverne amendment). This provision does not affect copyright ownership.
Unless copyright is transferred by contract or statute, it remains with the copyright holder.

Sharing and reuse
Other than for strictly personal use, it is not permitted to download, forward or distribute the text or part of it, without the consent of the author(s) and/or copyright holder(s), unless the work is under an open content license such as Creative Commons.

Takedown policy
Please contact us and provide details if you believe this document breaches copyrights.
We will remove access to the work immediately and investigate your claim.

This work is downloaded from Delft University of Technology.

Check for updates

IET Renewable Power Generation

WILEY

The Institution of Engineering and Technology

REVIEW OPEN ACCESS

Sub-Synchronous Oscillation Identification in Multi-Converter Energy Systems: Review and Assessment of Existing Signal Record-Based Methods

Camila Castrillón-Franco[1] | José Luis Rueda-Torres[1] | Arturo Román-Messina[2]

[1]Intelligent Electrical Power Grids, Delft University of Technology, Delft, The Netherlands | [2]Graduate Studies Program in Electrical Engineering, Cinvestav, Guadalajara, Mexico

Correspondence: Camila Castrillón-Franco (mcastrillonfra@tudelft.nl)

Received: 2 April 2026 | **Revised:** 18 June 2026 | **Accepted:** 8 September 2026

ABSTRACT

Oscillatory phenomena have been extensively studied in conventional power systems; however, the growing penetration of converter-based components—such as renewable generation, flexible alternating current transmission system (FACTS) devices, energy storage devices, electrolysers and high voltage DC (HVDC) transmission—has introduced new oscillation mechanisms, including sub-synchronous and super-synchronous oscillations (SSO), SSOs are specially critical in multi-converter (zero inertia) architectures, like offshore systems. Therefore, in this paper, a review and classification of SSO associated with converter-based devices, and a survey of existing methods for SSO assessment in multi-converter offshore systems, are presented. Finally, some signal record-based techniques are evaluated among the available identification methods, because they do not require a detailed analytical model of the system, which is often unavailable in systems with multiple converters. To assess these methods, three representative case studies are studied, highlighting their advantages and limitations. The results identify key challenges in reliably detecting and characterising oscillations in modern, evolving power systems.

1 | Introduction

In power system planning and operation, a key challenge is maintaining dynamic stability under external disturbances and changing operating conditions. This challenge has intensified with the increasing integration of renewable energy sources, due to their inherent variability, and the widespread deployment of converter-based technologies such as HVDC transmission systems and FACTS devices. This is particularly challenging in weak grids, where low frequency and minimal short-circuit radio make the voltage and frequency more susceptible to disturbances. Additionally, the operating point of renewable sources significantly influences system stability, especially since these systems typically lack surrounding synchronous generators to provide necessary support. While these technologies enhance system flexibility, they also introduce new dynamic interactions that can give rise to oscillatory phenomena across a wide frequency range. These include sub-synchronous oscillations (SSO) (whose frequency is below the nominal system frequency, but do not include electromechanical oscillations with frequencies of 0.1–2 Hz [1]) and super-synchronous oscillations (oscillatory frequencies between the nominal frequency and twice the nominal frequency), which differ from traditional inter-area and intra-area oscillations occurring in the 0–2 Hz range, both in frequency characteristics and underlying mechanisms [2]. Sub-synchronous oscillations can severely compromise power system operation, potentially leading to equipment damage and outages even under normal operating conditions.

Abbreviations: SSO, sub-synchronous oscillations; WPP, wind power plant; DMD, dynamic mode decomposition; FFT, fast fourier transformation.

This is an open access article under the terms of the Creative Commons Attribution-NonCommercial-NoDerivs License, which permits use and distribution in any medium, provided the original work is properly cited, the use is non-commercial and no modifications or adaptations are made.
© 2026 The Author(s). *IET Renewable Power Generation* published by John Wiley & Sons Ltd on behalf of The Institution of Engineering and Technology.

Sub-synchronous and super-synchronous oscillations have been observed in power systems since the 1970s [3]. Early occurrences were primarily attributed to sub-synchronous interactions (SSI) between the mechanical shaft systems of conventional synchronous generators and series-compensated transmission lines or HVDC links. Additional contributing factors include interactions between power plant control systems (PPSs) and series compensation, which can reduce torsional mode damping, as well as the fast dynamic response of synchronous generator controllers, such as power system stabilisers (PSSs) and governor control systems [4–7].

In recent years, numerous sub-synchronous and super-synchronous oscillation events involving converter-based devices have been reported in the literature [2, 8–10]. Notable examples include oscillations arising from interactions between type-3 wind power plants (WPPs) and series-compensated transmission lines. These events include the 2007 incident in Minnesota [2], where a 100 MW wind power plant operated radially through a series-compensated line; the 2009 South Texas event [2, 11, 12], in which the tripping of a transmission line resulted in multiple WPPs remaining connected to series-compensated lines; and several interactions between type-3 WPPs and double-circuit series-compensated transmission lines reported in the North China power system between 2012 and 2013 [2, 13].

Other reported oscillatory phenomena involve interactions between converter-based devices and weak grid conditions. Notable events include oscillations around 30 Hz observed in Xinjiang, China, between 2014 and 2015 [2, 14], where type-4 wind power plants (WPPs) interacted with a weak grid, ultimately leading to the tripping of a thermal power plant. Similar phenomena were reported at Hydro One in Canada [14, 15] in 2015, where the interaction between a 30 Mvar shunt capacitor and 10 MVA solar farms resulted in oscillatory behaviour. Additionally, generation oscillations at approximately 20 Hz and 9 Hz were observed in the Great Britain power system in 2019, attributed to interactions between offshore WPPs and weak grid conditions [16]. In this event, 1.1 million customers were disconnected from the system due to the interaction and subsequent disconnection of the 737 MW Hornsea offshore wind farm from the rest of the British system, leading to a large frequency drop outside the system.

These events demonstrate that multiple oscillation mechanisms can arise in power systems with converter-based devices, leading to wide variations in oscillation frequencies and durations that impact the performance of these devices, especially in offshore power systems. Such diversity must be carefully considered when developing strategies for reliably identifying oscillatory behaviour in measured power system signals.

To establish a consistent understanding of sub-synchronous and super-synchronous oscillations in power systems with high penetration of converter-based technologies, this paper reviews the various oscillation mechanisms reported in the literature and presents a state-of-the-art overview of the principal methods currently used for SSO identification. While recent studies have primarily focused on literature reviews and comparative analyses of existing approaches, this work evaluates several widely adopted signal record-based methods for parametric oscillation identification, with particular emphasis on the characteristics of SSO. The analysis aims to highlight the key challenges and outline directions for developing robust identification methods suitable for modern, evolving power systems.

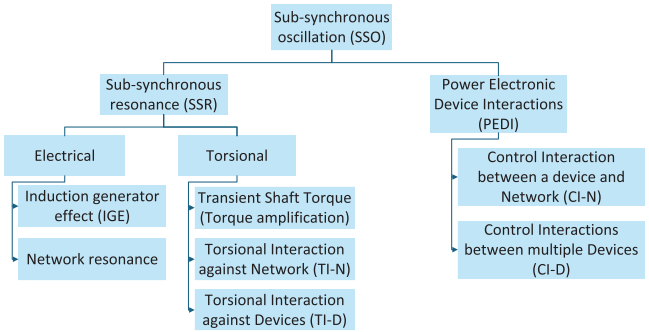


FIGURE 1 | SSO classification. Adapted from reference [1].

The rest of this paper is structured as follows. Section 2 provides background on sub-synchronous oscillation, including its classification and the identification methods available in the literature. Section 3 introduces the theoretical basis of the signal record-based methods proposed for application in Section 4 across three scenarios: a synthetic signal, a simulated study case, and a real case in which SSO in systems with multiple converters is reported. Finally, the conclusions and future work are summarised in Section 5.

2 | Recap of SSO Essentials Reported So Far

2.1 | SSO Classification

Although SSO oscillation phenomena have been reported in the literature since the 1970s, the mechanisms underlying these oscillations remain under study, particularly as new technologies that generate them have been incorporated into electrical power systems. Therefore, the classification of these oscillations is continually evolving to encompass all observed phenomena in real-world operating events. In the extension of the power system stability classification presented by [17], the SSO could be included under resonance stability and converter-driven stability, which are two new categories. However, in some cases, a sub-synchronous oscillatory phenomenon could overlap with both categories, since the first focuses on the mechanisms that lead to these phenomena, and the second mainly concerns the speed of the interaction. For that reason, CIGRE presented a classification of sub-synchronous oscillations, considering the underlying mechanisms and the devices involved in the oscillatory phenomena, as shown in Figure 1.

The sub-synchronous resonances (SSR) arise between the series-compensated capacitors installed in transmission lines and the generators, which also result in shaft failures [18, 19]. At the same time, these oscillations could be caused by electrical and torsional interactions. The electrical interaction could be generated by the induction generator effect or by network resonance. Induction generator effect (IGE) [19–21], happens when the rotors cause unexpected current growth in the armature terminals. When the rotor speed exceeds the rotating speed of the magnetic field

17521424, 2026, 1, Downloaded from https://ietresearch.onlinelibrary.wiley.com/doi/10.1049/rpg2.70375 by Technical University Delft, Wiley Online Library on [15/10/2026]. See the Terms and Conditions (https://onlinelibrary.wiley.com/terms-and-conditions) on Wiley Online Library for rules of use; OA articles are governed by the applicable Creative Commons License

generated by the current at the SSR frequency, the rotor resistance becomes negative, exciting oscillation. This type of oscillation occurs in systems with a high compensation rate. Network resonance is due to series compensation devices present in the system that act as an electrical resonance system that amplifies specific synchronous oscillations. This category includes series capacitor resonance, resonance in *LC* networks, such as underground cables or transformer inductances connected to line capacitances, and parallel resonance [22, 23].

The torsional resonances could be classified according to their underlying mechanisms. Transient shaft torque or torque amplification [4, 18] can occur in traditional power systems during large network disturbances, such as faults or device outages. The resulting interaction frequency between the internal generator fields is close to the generator shaft's natural frequency, leading to a significant swing in shaft torque. Torsional interaction (TI) [24, 25] is a phenomenon that includes electrical and mechanical interaction against the network or against devices. The interaction occurs when the resonance first generated in the network is transmitted to the turbine generator shaft, causing it to oscillate at its torsional frequency. If the induced sub-synchronous component in the generator's armature voltage has negative damping, the torsional oscillation can grow and damage the shaft and other generator components. The torsional interaction can also include the interaction between converter-based devices, involving the interaction between the masses in a generator (or wind turbine) and power-controlling devices, such as HVDC converters [26, 27], SVCs [28, 29], wind turbine control systems [30, 31], PSSs [32, 33], high-speed governor controls, and variable-speed drive converters. Among power-electronic devices, HVDC converters and SVCs are typically vulnerable to TI.

However, with the incorporation of converter-based devices, such as renewable sources, FACTS devices, Batteries, and HVDC lines, other mechanisms related to the control loops that cause SSO have emerged in power systems and are called Power Electronic Device Interactions (PEDI): In this category, interactions could be between a device and a network or among multiple devices. The control interaction between a device and network (CI-N) involves the interaction between the power electronics control system and other elements of the system, such as the series-compensated transmission line [34, 35], where a negative resistance is induced in the turbine at sub-synchronous frequencies, leading to SSO instability; if the system cannot adequately damp these oscillations, the generators may suffer severe damage. In essence, the oscillations caused by CI propagate more rapidly than those caused by SSR, owing to the controller's fast response. CI-N events have been frequently observed in type-3 WTGs with doubly fed induction generators (DFIGs). Nevertheless, CI-N can still occur even in systems without series compensation. These oscillations arise from interactions between the AC transmission network and either the DFIG or a direct-drive permanent-magnet synchronous generator (PMSG). In most offshore power systems, sub-synchronous control interaction can arise because permanent magnet synchronous generator (PMSG) wind turbines are typically employed and connected to the grid through full-scale power converters. As a result, there is no direct electromechanical interaction between the generator and the rest of the network; instead, oscillations are driven by interactions between the associated converter control systems and the grid, which is often weak.

The control interaction between multiple devices (CI-D) involves, however, two or more converter-based devices interacting with each other; each device acts both as a source of excitation and as a load seen by the other device. The instability arises from the closed-loop coupling between their control systems and may persist even in the absence of strong passive network resonance [36, 37]. Due to torsional interactions, these oscillations could occur between wind power plants and HVDC lines [36], wind power plants and STATCOMS [38], or HVDC and synchronous generators [39]. The main difference is that this kind of oscillation involves only the control loop, not the device's electromechanical elements.

2.2 | SSO Identification Methods

The literature reports several approaches for estimating the principal parameters of oscillatory modes, including the frequency and damping of sub-synchronous oscillations. These approaches include electromagnetic transient (EMT) simulations; analytical methods based on mathematical modelling and state-space linearization of the power system; impedance-based techniques—such as impedance scanning—for identifying oscillatory behaviour at specific locations within the system; and signal record-based methods that extract modal information directly from recorded system signals.

2.2.1 | EMT Simulations

EMT simulations are used for in-depth analysis of fast transient oscillations in power systems. Other methods, such as scanning methods, cannot account for all factors that affect the oscillation characteristics, such as the controllers of the power system devices under analysis, network topology, and several contingencies. For this reason, EMT simulations must be performed to get reliable results. The different electromagnetic and controller dynamics must be modelled to perform an EMT simulation, as they may influence sub-synchronous oscillations. The system can be tested for both small- and large-signal disturbances, and the most critical contingencies must be considered. Among the failures considered in this evaluation are 3-phase and 1-phase faults. In this type of simulation, significant effort is required to run them, making network equivalence techniques and parallel processing necessary. While EMT analysis is among the most accurate methods, a sophisticated EMT-level model is expensive and is generally used to validate results from other preliminary analyses. Compared with other techniques, the EMT method can simulate nonlinear dynamics and switching devices. However, it has some drawbacks: the simulation is time-consuming, additional methods are needed to determine oscillation metrics like frequency, damping, or phase, and it only provides signals in the time domain. This makes it impossible to identify the underlying mechanism or pinpoint the element responsible for the instability phenomena [9].

17521424, 2026, 1, Downloaded from https://ietresearch.onlinelibrary.wiley.com/doi/10.1049/rpg2.70375 by Technical University Delft, Wiley Online Library on [15/10/2026]. See the Terms and Conditions (https://onlinelibrary.wiley.com/terms-and-conditions) on Wiley Online Library for rules of use; OA articles are governed by the applicable Creative Commons License

2.2.2 | Analytic Methods

The small-signal stability assessment (SSA) is widely used to evaluate electromechanical oscillations in interconnected power systems, sub-synchronous oscillations among different types of oscillatory modes [40]. To perform this analysis, the model of the dynamic devices is first linearised at a specific operating point, and can be represented as a set of linear differential equations:

$$\dot{x} = Ax + Bu \tag{1}$$

where x and u indicate state and control variables, respectively. A linear state space is obtained by combining the different devices' linearised models; finally, the eigenvalues are calculated from the system's state matrix as [41]:

$$det(A - \lambda I) = 0 \tag{2}$$

where det indicates the determinant of a matrix, λ the eigenvalues, and I the identity matrix; if an eigenvalue within the sub-synchronous frequency range contains a positive real part, the damping at the frequency is negative, indicating that there would be a high potential SSO. Empirical studies indicate that these modelling approaches effectively characterise dynamic phenomena within the 0.1–50 Hz frequency range, making them well-suited for analysing SSO and sub-synchronous control interactions (SSCI) in modern power systems [42, 43]. This method can provide key oscillation characteristics, including frequency and damping, and can also be used to derive input-output transfer functions or reduced-order models. Unlike electromechanical oscillation analysis, the study of sub-synchronous oscillations requires detailed consideration of both network dynamics and generator stator behaviour; Therefore, the modelling framework for the analytical system must differ accordingly. When small signal analysis (SSA) is employed to assess electromechanical oscillations, the goal is to represent the slow evolution of system parameters. Consequently, certain dynamics are neglected, including the frequency response around the system's nominal frequency. In this approach, voltages and currents are represented by phasors, electromagnetic transients are disregarded, and the converter is modelled using an average model. Conversely, when the focus is on studying SSO, a different approach is required. In this case, a nonlinear model is used and linearised around an operating point, incorporating faster dynamics such as inner current loops, outer control loops, converter switching effects, and PLL dynamics [43, 44]. This enables analysis of a wide range of frequency phenomena, but also increases the model's complexity and the difficulty of analysis. Additionally, in some cases, such detailed models are unavailable or not fully developed by manufacturers [1].

One of the main drawbacks of this methodology is the need for a linearised model; therefore, it requires knowledge of the power system's parameters. However, large converter-based networks are complicated to characterise, and the models of some devices, such as wind turbines or HVDC lines, are black boxes in which manufacturers do not provide internal models.

To obtain the linearised model, there are two paths: the first is an overall approach, in which a nonlinear model of the entire grid, with state variables held constant at steady state, is built. A small-signal model in the format of a linear time-invariant (LTI) system is then obtained using numerical perturbation. In the second approach, a small-signal model is built block by block, assembling components into a network admittance for large-scale systems. Aggregation is then conducted to have a two-impedance system suitable for applying the generalised Nyquist stability criterion [2].

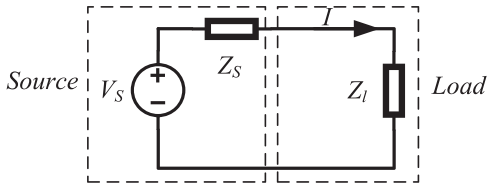


FIGURE 2 | Power system impedance representation [45].

2.2.3 | Impedance Scanning

Impedance scanning is nowadays a widely used method for initial power system assessment to identify sub-synchronous oscillations. Those methods aim to evaluate different scenarios, identify possible risks, and then submit to detailed studies. There are several screening methods; the most used are Impedance model-based analysis, radiality factor and unit interaction factor [1].

Impedance-based methods are widely used to assess oscillatory stability in a power network with many power electronic converters. The principle of this technique is to evaluate the impedance seen from a device and determine its stability based on the resonance frequencies and damping [45]. The system under study is divided into source and load subsystems. The source subsystem is modelled by its Thevenin equivalent circuit, consisting of an ideal voltage source (Vs) in series with an output impedance (Zs). In contrast, the load subsystem is modelled by its input impedance (Zl). This representation can be observed in Figure 2.

The impedance model around an operating point of a converter-based device can be represented by a transfer function $Z(s)$ and can be defined as:

$$Z(s) = \frac{U(s)}{I(s)} \tag{3}$$

There are several methods for calculating impedance. The first is passive frequency scanning, in which the main objective is to determine the electrical network's impedance as a function of frequency. In this process, the admittance matrix is formed at a specific frequency, and the equivalent impedance is computed using matrix-reduction techniques [1]. This method should be applied to a linear time-invariant system, since impedance model-based analysis is performed using the small-signal model.

For the reasons mentioned above, this method is used only to identify potential critical operating points; the identified points must then be evaluated in an EMT simulation. Also, it is essential to note that this stability analysis is a small-signal analysis around an equilibrium point.

17521424, 2026, 1, Downloaded from https://ietresearch.onlinelibrary.wiley.com/doi/10.1049/rpg2.70375 by Technical University Delft, Wiley Online Library on [15/10/2026]. See the Terms and Conditions (https://onlinelibrary.wiley.com/terms-and-conditions) on Wiley Online Library for rules of use; OA articles are governed by the applicable Creative Commons License

When the model of an electrical device, such as a wind generator park, is unavailable, dynamic frequency scanning can assess the stability of the existing black-box model [46]. The electrical system and device frequency are obtained from EMT simulations, assuming stable operation conditions and using a detailed time-domain representation [9, 47]. With this technique, a small signal voltage or current is injected into the system before its impedance is determined. Voltage injection creates a smaller disturbance than current injection because, in general, the system is less sensitive to voltage perturbations; however, with current injection, it is possible to capture the impact of other devices on the system side [48].

The impedance model could be built in the dq [46, 49] or abc [50–52] reference frames. To assess the stability in the impedance scanning model, it is possible to apply the following criteria: (i) resistance analysis (using the real part of the impedance model), (ii) Bode plot, and (iii) Nyquist's stability criteria.

To apply the Nyquist stability criterion, it is first necessary to obtain the impedance models of the converter-based device and the equivalent power system, assuming the converter voltage is stable and the power system is stable when the power system impedance is zero [53]. This system can be analysed as a feedback system, and the root-locus method and Nyquist criterion can be applied in the open loop. The system is stable if the eigen loci do not encircle (−1,0). Similarly, in Bode plots, the oscillation frequency is detected at the point where two impedances have opposite phases, and the gain should be less than 1 when the phase shift is stable [50].

To assess stability in a network with multiples voltage and current sources, a frequency domain method based on the nodal admittance matrix is used with the generalised Nyquist criterion (GNC) [51]; this approach needs less information about the system, but only determine the system stability based on the open-loop function and the result depends on the way the system is split, sometimes, the misleading associations could generate right-hand plane poles [52]. Other drawbacks of these methods are that they do not allow analysis of the effects of specific control parameters on system stability, and it is challenging to locate the origin of the modes.

2.2.4 | Signal Record-Based Methods

Methods based on measurements use data from local measurements or from additional devices, such as PMUs or other measuring elements installed in the power system. EMT software is used to create and simulate these conditions in the academy and industry, generating the data sets necessary to apply these methodologies.

These methods are characterised by calculating the main features of the signals over a predetermined time interval. However, before applying any method, preprocessing is required; the first step is event segmentation, which determines the oscillation's start and end points. For this step, time resolution is essential, as some identification methods require a minimum number of signal samples or a sample window.

In general, for the implementation of any signal record-based methods, it is required to fulfil the Nyquist criterion, which establishes that a signal can only be reconstructed if the sampling frequency f_s is:

$$f_s > 2f_{max} \tag{4}$$

where f_{max} is the frequency that will be identified [54, 55]. In the specific case of the SSO, the maximum frequency of the super-synchronous component is $2f_{nom}$, where f_{nom} is the nominal frequency of the system. However, when the signal is obtained, for instance, from a PMU, this criterion may not be met depending on the reporting rate. Additionally, these methods require a minimum number of signal samples (or an observation window) because the oscillatory parameters—such as frequency, damping, amplitude, and phase—must be inferred from the temporal evolution of the measured data. A short data window provides insufficient information to uniquely distinguish these parameters, leading to poor identifiability and sensitivity to measurement noise. In particular, frequency estimation requires observing enough oscillation cycles to resolve periodic behaviour, while damping estimation generally needs a longer window because it depends on detecting gradual changes in the oscillation envelope. In subspace and modal identification methods, such as DMD, prony, or Matrix Pencil, a sufficient number of samples is also necessary to construct data matrices with adequate rank and numerical conditioning for reliable parameter estimation [56, 57].

In signal processing terms, segmentation is the process of identifying groups of data segments that possess similar properties [58]. The second step is the filtering to remove both the fundamental frequency and other frequency bands that are not of interest for further analysis [59, 60].

After preparing the data, several methods in the literature are available for oscillation identification, which can be classified by domain: time-domain, time-frequency, and frequency.

In the time-domain method, the prony method is widely used as a benchmark for comparing other approaches, in which data samples are fitted to an exponential model [61]. Other approaches include the eigensystem realisation algorithm (ERA), the matrix pencil, the estimation of signal parameters via rotational invariance techniques (ESPRIT), particle swarm optimisation, and some autoregressive methods, such as the Kalman filter, Yule–Walker, and recursive least squares (RLS), among others [62]. In [63], three different data-driven methods, prony analysis, matrix pencil, and ERA, are used to identify power system eigenvalues from measurement data and obtain a reduced-order system model. These methods require instantaneous or PMU measurements (e.g., voltage, current, active or reactive power) as inputs, but are computationally intensive and also require the number of modes as input. Also, their observability is poor; they need more time (several SSO cycles) and an adequate signal selection to achieve SSO, which can make them impractical for real-time applications.

In [64, 65], auto regressive moving average (ARMA) methods have been implemented to identify the oscillations in the power system with the incorporation of wind power plants. The novelty of implementing these methods lies in incorporating environmen-

17521424, 2026, 1, Downloaded from https://ietresearch.onlinelibrary.wiley.com/doi/10.1049/rpg2.70375 by Technical University Delft, Wiley Online Library on [15/10/2026]. See the Terms and Conditions (https://onlinelibrary.wiley.com/terms-and-conditions) on Wiley Online Library for rules of use; OA articles are governed by the applicable Creative Commons License

tal noise and the converters' dynamics, thereby demonstrating robustness against it. However, autoregressive methods are biased for short data, assume stationary signals, which is not the case in regular power system operation, and incur high computational costs.

In the frequency domain, the most commonly used method is the fast Fourier transform (FFT) [66], which decomposes signals into sinusoidal components with different frequencies. To apply this method, a large window size is used to obtain the data of interest. Still, the signal's time-varying conditions and damping characteristics cannot be obtained. Also, the method's accuracy depends on the window length, and it cannot suppress time-varying noise. For these reasons, several modifications have been implemented to improve this method. For instance, in [67], a sliding window is used to avoid frequency leakage and the fence effect, and in [68], an interpolation FFT algorithm and a transient energy flow method are used for online monitoring of sub-synchronous oscillations via a phasor measurement unit (PMU). A general disadvantage of the methods mentioned is that a relatively long window is required; otherwise, spectral resolution is low, and frequency determination is error-prone. In addition, a change in the oscillation frequencies may be detected, but there is no indication of when it occurred, and it may take a while for the new frequency to become visible in the spectrum. Due to the drawbacks of the FFT method, several other Fourier-based techniques have been developed, including the periodogram [69], Welch's method [70], and frequency response functions [71]. The advantage of those methods is that the resolution is adjustable and leakage is lower than with only an FFT, thereby increasing the accuracy of the results.

Finally, in the time-frequency domain, the most well-known methods are the Hilbert-Huang transform (HHT), which utilises empirical mode decomposition (EMD), and the wavelet transform. In [72], the Hilbert transformation is first applied to obtain the instantaneous parameters, and then the damping ratio is calculated for every model component. However, this method could yield misleading oscillation parameters, leading to modal aliasing. Various applications of the wavelet transform have been proposed, including its use in signals obtained from phasor measurement units [73, 74] as well as the application of wavelet-based nonlinear mode decomposition, which promises to enhance the characterisation of time-evolving SSOs [75].

In this category, the short-time Fourier transform (STFT) is also included, which is a method that segments the signal into short-time windows and performs an FFT on each window; the parameters are then estimated from the resulting spectrogram [76]. Variational mode decomposition (VMD) is another promising, adaptive, data-driven technique. However, it requires prior specification of the number of modes and manual tuning of penalty parameters, thereby limiting its suitability for analysing rapidly evolving oscillations in which mode interactions may give rise to new dynamic behaviours [77]. When combined with other methods, such as prony analysis or recursive linearization, VMD's predictive capability can be significantly enhanced.

The rapid evolution of these methodologies has been marked by recent advancements in wavelet and Fourier analysis, which have contributed to the emergence of nonlinear mode decomposition techniques. These advanced approaches enable analysis of nonlinear and nonstationary system dynamics and identification of phase synchrony in empirical data [75]. Additionally, promising developments include enhanced VMD methods combined with nonlinear least-squares fitting, which have proven effective at isolating SSOs in wind-integrated power systems [78]

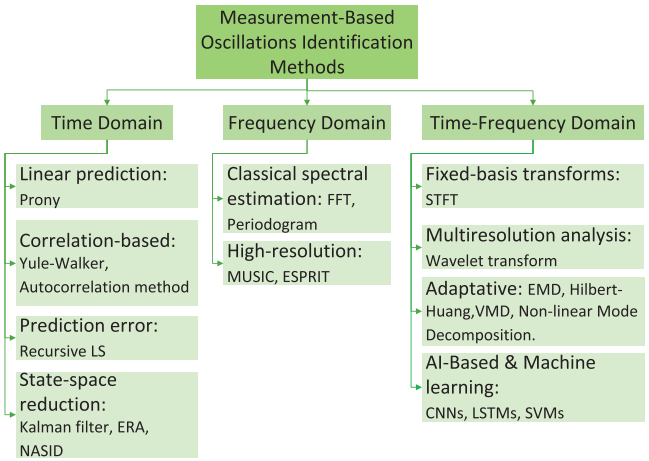


FIGURE 3 | Measurement-based method classification.

In Figure 3, the classification of the measurement-based methods and some examples are presented.

2.2.5 | Emerging Methods

Several data-driven artificial intelligence methods have been proposed to extract information about SSO in power systems. For instance, a machine learning method based on multiple support vector machines is proposed in [79]. In this work, a large dataset of field PMU data is analysed, and three SSO-related features are extracted. An automatic update function based on incremental learning is also developed. In [80], a fast reduced kernel extreme learning machine (RKELM) model is used to extract oscillation features. This research examined the possibility of super-synchronous components in the oscillation signal and the limitations of PMU-recorded measurements, which are filtered to obtain signals associated with the system's fundamental frequency; however, this method applies only to DFT-based synchrophasors. Other machine learning algorithms used for SSO identification include transfer component analysis (TCA) [81], broad learning system [82], and a joint distribution adaptive transfer learning method [83], among others.

With the development of new measurement devices, it is possible to obtain time-synchronised waveform measurements from different locations of a power system through a waveform measurement unit (WMU). With the WMU likely to receive raw time-domain data for power system variables such as voltage and current, the sampled data are precisely time-stamped, allowing them to be time-synchronised. One application of these measurement units is the identification of sub-synchronous and super-synchronous oscillations in a wind farm, thereby avoiding the picket-fence effect of Fourier analysis associated with PMUs [84]. With this newly available information, new methods

17521424, 2026, 1, Downloaded from https://ietresearch.onlinelibrary.wiley.com/doi/10.1049/rpg2.70375 by Technical University Delft, Wiley Online Library on [15/10/2026]. See the Terms and Conditions (https://onlinelibrary.wiley.com/terms-and-conditions) on Wiley Online Library for rules of use; OA articles are governed by the applicable Creative Commons License

have been developed to detect and classify events; in [85], a Lissajous-based method is proposed for event classification via image processing using a convolutional neural network (CNN) to correctly identify the event. The drawbacks of these methods are the limited number of WMUs installed in the actual monitoring system and the large volume of data to be analysed, as these measurement units record 256 samples per cycle.

3 | Assessment of Signal Record-Based Methods

From Section 2.2, it can be concluded that signal record-based methods are widely used to identify different oscillations in converter-based power systems. These methods have the advantage of not requiring a detailed analytical model of the system, which is often unavailable due to intellectual property rights held by converter equipment developers. Additionally, such methods can be applied during the project design phase using simulated signals, as well as during operation, utilising measurement data obtained from the system. To evaluate their main advantages and challenges in accurately identifying SSO characteristics, some of the most representative signal-record methods from each category shown in Figure 3 are examined. This includes frequency-domain methods such as the fast Fourier transform (FFT), time-domain methods such as prony and dynamic mode decomposition (DMD), and the wavelet transform, which is a time-frequency method.

3.1 | Theoretical Background

3.1.1 | FFT

The FFT is an efficient algorithm for computing the discrete Fourier transform (DFT). It converts a discrete time-domain signal into its frequency-domain representation [86].

To obtain the frequency-domain representation of discrete data, the discrete Fourier transform is applied. Given a discrete signal consisting of N samples, $x[0], x[1], \ldots, x[N-1]$, the DFT is defined as:

$$X[k] = \sum_{n=0}^{N-1} x[n] e^{-j2\pi kn/N}, \qquad k = 0, 1, \ldots, N-1. \tag{5}$$

The DFT measures how much of a sinusoid of frequency k/N (relative to the sampling rate) is present in the signal. The output $X(k)$ of the FFT is a sequence of complex numbers. The magnitude of each coefficient is computed as:

$$|X[k]| = \sqrt{(\Re[X[k]])^2 + (\Im[X[k]])^2}. \tag{6}$$

The magnitude spectrum displays the strength of each frequency component. Let f_s be the sampling frequency and N the number of samples. Then the frequency represented by index k in the FFT is:

$$f_k = \frac{k}{N} f_s. \tag{7}$$

Thus, peaks in the magnitude spectrum indicate the signal's dominant frequencies. The frequency resolution of the FFT is given by:

$$\Delta f = \frac{f_s}{N}. \tag{8}$$

A higher resolution (i.e., a smaller Δf) requires a larger N, meaning more data points. Windowing functions (such as the Hann and Hamming windows) are used to reduce spectral leakage, thereby improving the accuracy of frequency identification.

Additionally, for non-stationary signals, the short time Fourier transform (STFT) was developed [87], a fundamental tool in time-frequency analysis that characterises the spectral content of signals whose frequency components vary over time. Unlike the classical Fourier transform, which assumes stationarity over the entire observation interval, the STFT enables localised frequency analysis by introducing temporal segmentation [88].

Let $x(t) \in L^2(\mathbb{R})$ be a finite-energy signal and let $w(t) \in L^2(\mathbb{R})$ be a real-valued window function with compact or effectively compact support. The STFT of $x(t)$ with respect to $w(t)$ is defined as:

$$\mathrm{STFT}_x(t, \omega) = \int_{-\infty}^{\infty} x(\tau)\, w(\tau - t)\, e^{-j\omega\tau}\, d\tau$$

where $t \in \mathbb{R}$ denotes the time shift and $\omega \in \mathbb{R}$ denotes the angular frequency.

For each fixed time parameter t, the STFT corresponds to the Fourier transform of the signal weighted by a window centred at time t. As the window slides along the time axis, the STFT captures the local spectral behaviour of the signal. The magnitude $|\mathrm{STFT}_x(t, \omega)|$ represents the contribution of frequency ω at time t, while the phase contains information about local signal structure.

To visualise the STFT, the spectrogram is defined as the squared magnitude of the STFT:

$$S_x(t, \omega) = |\mathrm{STFT}_x(t, \omega)|^2$$

And provides a non-negative time–frequency energy distribution.

The temporal width of the window function $w(t)$ determines the resolution properties of the STFT. A narrow window yields high temporal resolution at the expense of frequency resolution, while a wide window improves frequency resolution but degrades temporal localisation. This trade-off is a manifestation of the time–frequency uncertainty principle.

Since signal analysis involves available data samples, it requires a discrete-time application. In the discrete-time setting, let $x[n]$ be a sampled signal and $w[n]$ a finite-length window. The discrete STFT is given by

$$\mathrm{STFT}_x(m, k) = \sum_{n=-\infty}^{\infty} x[n]\, w[n-m]\, e^{-j2\pi kn/N}$$

17521424, 2026, 1, Downloaded from https://ietresearch.onlinelibrary.wiley.com/doi/10.1049/rpg2.70375 by Technical University Delft, Wiley Online Library on [15/10/2026]. See the Terms and Conditions (https://onlinelibrary.wiley.com/terms-and-conditions) on Wiley Online Library for rules of use; OA articles are governed by the applicable Creative Commons License

Where m denotes the time index, k the frequency bin index, and N the number of frequency samples.

3.1.2 | Prony

Prony's method is a classical technique for estimating the parameters of a signal that can be modelled as a sum of damped complex exponentials. Given a finite set of uniformly spaced samples, the method recovers the amplitudes, damping factors, and frequencies of the exponential components [89].

Assume the discrete-time signal has the form:

$$x[n] = \sum_{k=1}^{M} A_k e^{(\alpha_k + j\omega_k)n},$$

Here,

- A_k are complex amplitudes,
- α_k are damping factors,
- ω_k are angular frequencies,
- z_k are the complex exponential poles.

Given the samples $x[0], x[1], \ldots, x[N-1]$, the goal is to estimate $\{A_k, z_k\}_{k=1}^{M}$.

The signal satisfies a linear recurrence equation:

$$x[n] + a_1 x[n-1] + a_2 x[n-2] + \cdots + a_M x[n-M] = 0.$$

The coefficients $a_1, \ldots, a_M$ are obtained by solving a linear system constructed from the data samples.

Define the prediction polynomial:

$$P(z) = z^M + a_1 z^{M-1} + a_2 z^{M-2} + \cdots + a_M.$$

The roots of $P(z)$ give the poles z_k, from which damping factors and frequencies are extracted:

$$\alpha_k = \ln |z_k|, \qquad \omega_k = \arg(z_k).$$

Once the poles z_k are known, the amplitudes A_k are found by solving the system.

$$x[n] = \sum_{k=1}^{M} A_k z_k^n,$$

for $n = 0, 1, \ldots, M-1$, typically using least squares if more samples are available.

3.1.3 | DMD

DMD is a data-driven method initially developed in fluid dynamics and later extended to other areas to identify spatio-temporal coherent structures (modes) and their associated frequencies and growth/decay rates directly from time-series data [90–92]. Unlike other time-domain methods that require impulse response information, DMD works directly with sequential snapshots of the system state.

To apply DMD, it is required to follow the steps presented below:

1. **Snapshot Data**: Collect a sequence of state measurements (snapshots) of the system at equally spaced times:

$$X = \begin{bmatrix} x_1 & x_2 & \cdots & x_{m-1} \end{bmatrix}, \quad X' = \begin{bmatrix} x_2 & x_3 & \cdots & x_m \end{bmatrix} \tag{9}$$

   where $x_k \in R^n$ is the system state at time $k\Delta t$.

2. **Linear Mapping Approximation**: Assume a linear operator A that advances the state in time:

$$x_{k+1} \approx Ax_k, \qquad X' \approx AX \tag{10}$$

3. **Low-Rank Approximation (SVD)**: Apply singular value decomposition to X:

$$X = U\Sigma V^T \tag{11}$$

   Truncate to rank r to reduce noise and focus on dominant dynamics.

4. **Reduced Operator**: Project A onto the subspace spanned by U_r:

$$\tilde{A} = U_r^T X' V_r \Sigma_r^{-1} \tag{12}$$

5. **Eigenvalue Decomposition**: Compute eigenvalues and eigenvectors of $\tilde{A}$:

$$\tilde{A}W = W\Lambda \tag{13}$$

   where $\Lambda = \text{diag}(\lambda_1, \ldots, \lambda_r)$ contains the DMD eigenvalues.

6. **DMD Modes**: The spatial modes associated with each frequency are given by:

$$\phi_i = U_r W_i \tag{14}$$

   where W_i is the i-th eigenvector.

With both methods, the continuous-time poles are obtained as:

$$s_i = \frac{\ln(\lambda_i)}{\Delta t} \tag{15}$$

Using the eigenvalues λ_i obtained from the estimated matrix A. From $s_i = \sigma_i + j\omega_{di}$, the natural frequencies and damping ratios are:

$$\omega_{n,i} = \sqrt{\sigma_i^2 + \omega_{di}^2}, \qquad \zeta_i = -\frac{\sigma_i}{\omega_{n,i}} \tag{16}$$

17521424, 2026, 1, Downloaded from https://ietresearch.onlinelibrary.wiley.com/doi/10.1049/rpg2.70375 by Technical University Delft, Wiley Online Library on [15/10/2026]. See the Terms and Conditions (https://onlinelibrary.wiley.com/terms-and-conditions) on Wiley Online Library for rules of use; OA articles are governed by the applicable Creative Commons License

3.1.4 | Wavelet

The wavelet method is a mathematical technique used to analyse signals with components that vary over time. Unlike the Fourier transform, which provides only global frequency information, the wavelet transform offers a joint time-frequency representation, allowing localised analysis of transients, discontinuities, and non-stationary behaviour.

A *wavelet* is a function $\psi(t)$ with zero mean and compact support, which is scaled and translated to probe the signal at different resolutions [93].

$$\psi_{a,b}(t) = \frac{1}{\sqrt{|a|}}\psi\left(\frac{t-b}{a}\right),$$

where a is the *dilatation* in time and b is the *translation* in time.

The continuous wavelet transform of a signal $x(t)$ is defined as:

$$W_x(a,b) = \int_{-\infty}^{\infty} x(t)\frac{1}{\sqrt{|a|}}\psi\left(\frac{t-b}{a}\right)dt. \tag{17}$$

where $\psi(t)$ is the mother wavelet, a is the dilatation scale, b is the time scale, and $\psi\left(\frac{t-b}{a}\right)$ are the daughter wavelet function. The result $W_x(a,b)$ represents the contribution of scale a (frequency) at time location b. Smaller scales correspond to higher frequencies, while larger scales correspond to lower frequencies.

Different approaches have been proposed in the literature for the identification of oscillation parameters using continuous and discrete wavelet transforms. In the methodology proposed in [94], the real part of the ith mode is estimated as the slope of straight line portions of the logarithm of the CWT modulus:

$$ln|W_x(a,b)| = \alpha_i \tag{18}$$

And the imaginary part, which represents the natural frequency of the ith mode, is estimated from the slope of the phase of the CWT:

$$arg[W_x(a,b)] = \omega_i t + \theta_i \tag{19}$$

Then, the frequency and damping ratio of the ith mode are given by:

$$f_i = \frac{\omega_i}{2\pi}, \qquad \zeta_i = -\frac{\alpha_i}{\sqrt{\alpha_i^2 + \omega_i^2}} \tag{20}$$

4 | Application and Evaluation of the Identification Methods

4.1 | Synthetic Signals Analysis

To assess the performance of the measurement-based methods for SSO identification, the first case is a synthetic signal with characteristics described in the literature for SSO in converter-based systems. The signal used for this purpose consists of the 50 Hz fundamental component and two oscillatory modes, each

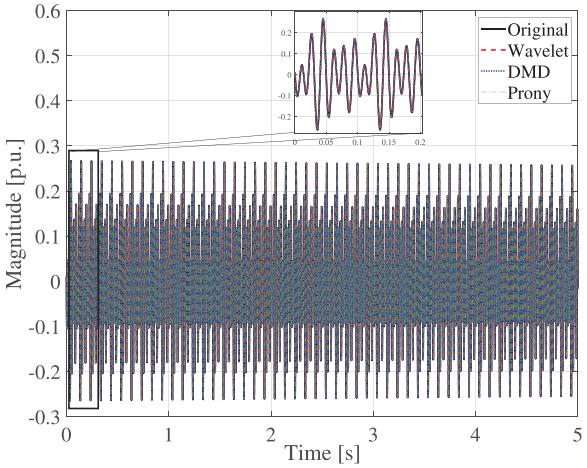


FIGURE 4 | Synthetic signal without noise and its reconstruction using the signal record-based methods.

with its own set of parameters. For the fundamental component, the used values are $A_1 = 0.05$, $f_1 = 50$ Hz, 1 = -1.3.

For the sub-synchronous component, the parameters selected are $A_{sub} = 0.08$, $\zeta_{sub} = 0.01\ s^{-1}$, $f_{sub} = 40$ Hz, $\varphi_{sub} = 0.75$ and for the super-synchronous component the parameters are $A_{sup} = 0.15$, $\zeta_{sup} = 0.009\ s^{-1}$, $f_1 = 60$ Hz, $\varphi_1 = 2$. The original and the reconstructed signals using the prony, DMD, and wavelet methods are presented in Figure 4.

When employing all measurement-based methods, the reconstructed signals closely match the original signals, as anticipated, because the original signals are noise-free and stable over time. However, this scenario is idealised; in practical situations, particularly in converter-based power systems, measurements are affected by noise from various devices and contain high-frequency components arising from converter switching. Additionally, the system's operating point continually fluctuates due to renewable energy variability and load changes.

Because multiple factors can affect measurements in a power system, two sensitivity analyses were conducted. The first analysis incorporates a noise component into the signal, as shown in Equation (21), thereby modifying the initially described signal.

$$y(t) = x(t) + n(t) \tag{21}$$

where $y(t)$ is the noisy signal, $x(t)$ is the original signal and $n(t)$ is the noise. The noise $n(t)$ has a Gaussian distribution, and each sample is defined from a Gaussian (normal) distribution:

$$n(t) \sim N(0, \sigma^2) \tag{22}$$

where 0 is the mean, and σ^2 is the variance related to the noise power and is defined in the form:

$$\sigma = \sqrt{\frac{A_{signal}^2}{10^{\frac{SNR}{10}}}} \tag{23}$$

where A_{signal} is the signal amplitude and SNR is the signal-to-noise ratio. In this case, the SNR is 30 dB, as reported in diverse

17521424, 2026, 1, Downloaded from https://ietresearch.onlinelibrary.wiley.com/doi/10.1049/rpg2.70375 by Technical University Delft, Wiley Online Library on [15/10/2026]. See the Terms and Conditions (https://onlinelibrary.wiley.com/terms-and-conditions) on Wiley Online Library for rules of use; OA articles are governed by the applicable Creative Commons License

TABLE 1 | Sub-synchronous oscillation identified by using the instantaneous signals recorded.

	Prony		DMD		Wavelet	
Methods Component	**Freq. [Hz]**	**Damp. [%]**	**Freq. [Hz]**	**Damp. [%]**	**Freq. [Hz]**	**Damp. [%]**
Sub	40.001	0.005	40.000	0.004	40.001	0.007
% Error	0.001	30.690	0.000	0.531	0.002	86.895
Super	60.000	0.0028	60.000	0.002	59.998	0.0028
% Error	0.000	17.286	0.000	0.531	0.003	16.226

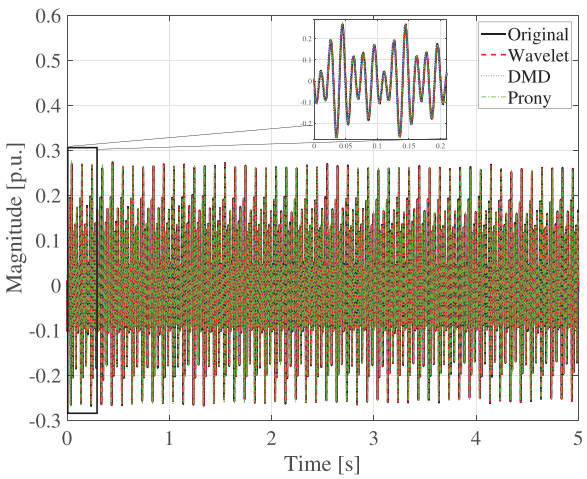


FIGURE 5 | Synthetic signal with noise and the reconstruction using the signal record-based methods.

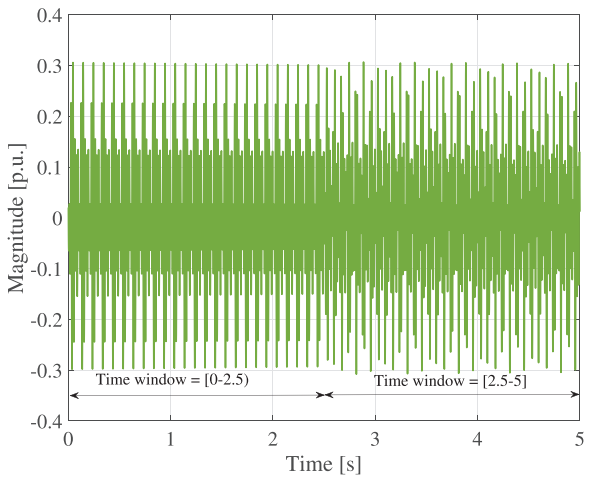


FIGURE 6 | Synthetic signal with parametric changes at t = 2.5 s.

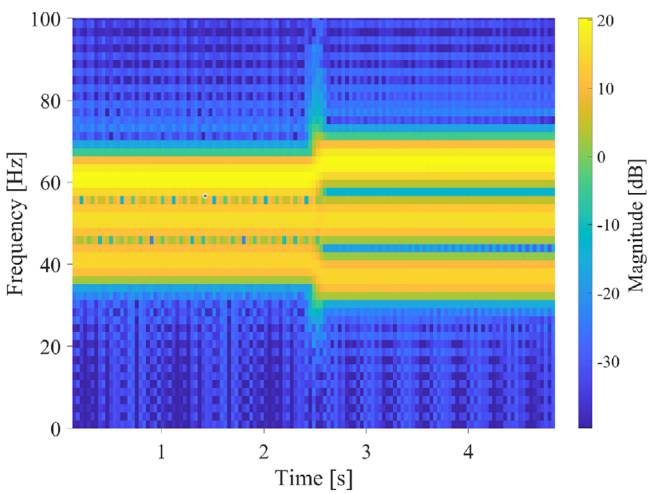


FIGURE 7 | Short-time frequency transform applied to a synthetic signal.

PMU data studies [95]. The original and the reconstructed signals with noise components are presented in Figure 5.

Table 1 shows the frequencies and damping identified using the presented methods. While the proposed techniques accurately identified the frequency, the damping values exhibited higher error rates, particularly with the prony and wavelet methods. The primary goal of the wavelet method is to reconstruct a specific signal by removing noise and to detect variations in frequency, damping, or energy over time. Therefore, when applying the CWT, filtering was unnecessary for identification. Conversely, the prony and DMD methods required a prefiltering step to preserve frequencies below 100 Hz and enhance accuracy. Nonetheless, the damping results from this method are less precise because they rely on a fitting process that can introduce errors.

The second sensitivity includes a change in the frequency and damping parameters of the sub-synchronous and super-synchronous components added to the signal at 2.5 s. The new values of the components are: for the sub-synchronous component $\zeta_{sub} = 0.01s^{-1} * 0.95$, $f_{sub} = 40Hz * 0.9$ and for the super-synchronous component, the parameters are $\zeta_{sup} = 0.009s^{-1} * 0.95$, $f_1 = 85Hz * 1.1$. The remaining values are the same as those presented previously. The synthetic signal with a change in the oscillation components at t = 2.5 s is presented in Figure 6.

To present the changes in the signal's parameters, the STFT was applied, and the system's frequency response over time, the spectrogram, is presented in Figure 7. In the figure, at $t = 2.5$ s, the frequency of the sub-synchronous and super-synchronous components changed by 5%, while the fundamental frequency remained unchanged as expected.

Using the three presented methods, the oscillations have been identified over a 5-s time window, and the results are presented in Table 2.

The three methods identified changes in the mode; however, the prony and DMD methods cannot determine the exact timing of

17521424, 2026, 1, Downloaded from https://ietresearch.onlinelibrary.wiley.com/doi/10.1049/rpg2.70375 by Technical University Delft, Wiley Online Library on [15/10/2026]. See the Terms and Conditions (https://onlinelibrary.wiley.com/terms-and-conditions) on Wiley Online Library for rules of use; OA articles are governed by the applicable Creative Commons License

TABLE 2 | Sub-synchronous oscillation identified by using the instantaneous signals recorded by changing the oscillation parameters.

Case	Methods Component	Prony		DMD		Wavelet	
		Freq. [Hz]	Damp. [%]	Freq. [Hz]	Damp. [%]	Freq. [Hz]	Damp. [%]
t < 2.5 s	Sub	39.976	0.001	41.332	0.062	40.000	0.007
	% Error	0.060	65.819	3.331	1460.7	0.000	66.100
	Super	60.009	0.008	60.652	0.010	59.999	0.0027
	% Error	0.015	264.4	1.087	344.01	0.001	14.446
t >= 2.5 s	Sub	36.001	0.004	36.446	0.008	36.000	0.002
	% Error	0.003	0.002	1.240	111.909	0.001	52.708
	Super	63.991	0.001	64.249	0.003	64.003	0.002
	% Error	0.014	52.691	0.388	79.773	0.004	12.784

these parameter changes, as they treat oscillations as stationary. Consequently, the percentage error in the estimated damping exceeds 100% because the analysis considers the entire signal over the time window. Using the wavelet method, the percentage error is small, and the time of the change can be identified. However, the main goal of this method is to reconstruct the signal and filter out the noise; for this reason, it is not the most accurate for calculating frequency and damping. One possible way to address these drawbacks is to first determine the optimal time windows using the wavelet method or the STFT, and then apply one of the available ringdown methods, such as prony's method. An important insight from these results is that estimating damping is generally more challenging than determining frequency, because frequency is primarily governed by the oscillation's phase evolution. In contrast, damping depends on the change in amplitude over time, resulting in smaller relative variations compared to the overall signal amplitude. In practice, amplitude changes are susceptible to noise, disturbances, and limited data length. Observing amplitude evolution typically requires several seconds due to slow damping; however, if this time window is too long, the oscillation may no longer be present in the system. Additionally, many power system oscillations, especially the SSO, have small damping ratios, making amplitude variations comparable to measurement noise.

4.2 | SSO in a Converter-Based System

The second case study presented to assess the trustworthiness of the measurement-based methods is a converter-based system comprising a wind power plant connected to an infinite bus. The one-line diagram of the system is shown in Figure 8. The system was adapted from the example available in [96], consisting of a 2.5 MVA wind power plant connected to the 220 kV infinite bus via a step-up transformer.

The wind power plant model is also presented in Figure 8, and it is modelled as a wind turbine connected to a permanent magnet synchronous generator (PMSG), which, in turn, is connected to a full-scale power electronic converter. The machine side converter (MSC) is a controller whose primary objective is to control the torque reference using the maximum power point tracker (MPPT) output as the electrical torque reference. The system is implemented in RSCAD for real-time simulation [96]. For the grid side converter (GSC), a grid-following converter is implemented, whose primary goals are to regulate the AC Voltage, reactive power, and DC Voltage. In this system, the main type of oscillation is SSO due to the interaction between the GSC and the equivalent impedance of the infinite system, especially when the system's SCR is below 5, indicating its weakness [97].

TABLE 3 | Sub-synchronous oscillation parameters identified by using the RMS recorded signals in the simulated system with different wind speed values.

Wind speed [m/s]	Prony		DMD	
	Freq. [Hz]	Damp. [%]	Freq. [Hz]	Damp. [%]
11	5.941	26.110	5.909	26.142
11.5	5.608	1.814	5.663	16.484
11.7	5.412	13.395	5.433	12.416
11.9	5.047	6.211	5.153	5.824
12	4.627	0.811	4.915	0.683

The SSO is excited by changing the AC Voltage reference of the GSC, from 1 to 0.9 p.u. at 0.3 s, when the SCR of the equivalent system is 0.68. This perturbation is applied to the system at different wind speeds, ranging from 12 m/s (the system's nominal value) to 11 m/s. The recorded active power generated by the wind power plant for the five analysed cases is presented in Figure 9, showing that as wind speed increases, the oscillation generated by the change in voltage reference has greater amplitude and duration, where even in cases with a lower SCR level, the system can be unstable.

To obtain the SSO parameters in the system, the DMD and prony methods are used, as they perform better when the oscillation is stationary, as in this case, where the only change is applied at 0.3 s, and the rest of the system's parameters remain constant. The results are presented in Table 3, showing that not only does the damping decrease, but also the oscillation frequency decreases as the wind speed increases.

However, in the operation of renewable energy sources, the primary source, which is wind, is not constant, and its speed

17521424, 2026, 1, Downloaded from https://ietresearch.onlinelibrary.wiley.com/doi/10.1049/rpg2.70375 by Technical University Delft, Wiley Online Library on [15/10/2026]. See the Terms and Conditions (https://onlinelibrary.wiley.com/terms-and-conditions) on Wiley Online Library for rules of use; OA articles are governed by the applicable Creative Commons License

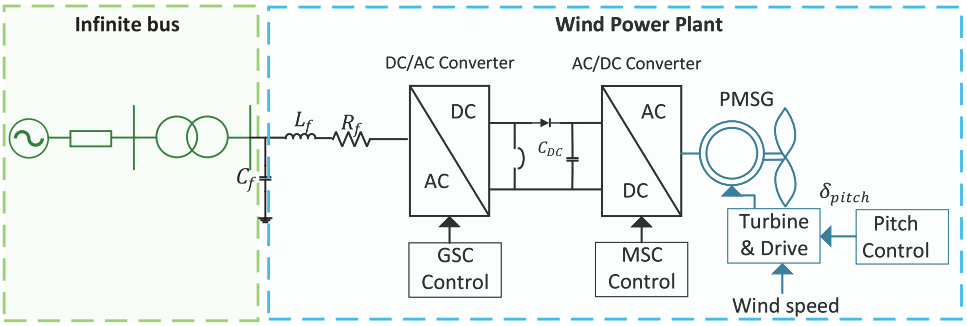


FIGURE 8 | Wind power plant connected to an infinite bus.

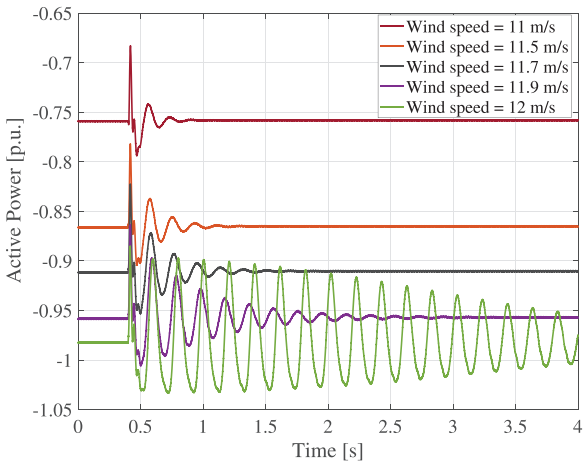


FIGURE 9 | Active power of WPP under wind speed changes.

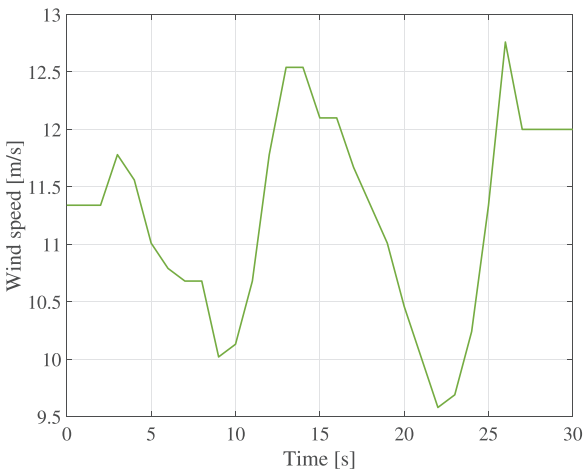


FIGURE 10 | Wind speed profile obtained from [98].

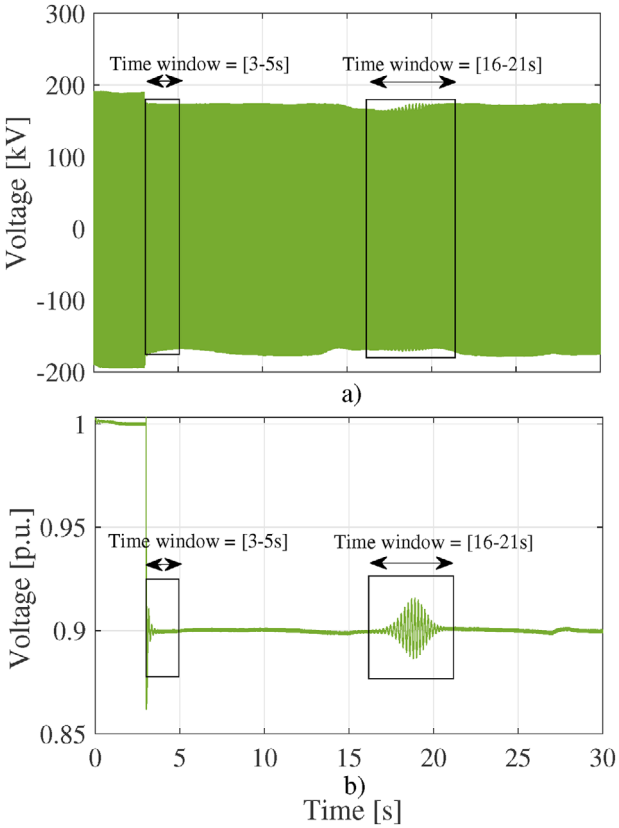


FIGURE 11 | Voltage of the infinite bus system with a wind speed profile. (a) Phase A instantaneous signal; (b) RMS signal.

varies, which in turn causes the power generated to vary over time. To assess the SSO's behaviour under generation variability, a wind speed profile is used as input to the wind turbine. The wind profile corresponds to measurements obtained and utilised in [98] and is presented in Figure 10.

As in the previous case, the AC voltage reference is changed at $t = 0.3$ s immediately after the wind speed profile is entered into the wind turbine. The voltage response is presented in Figure 11, where both the instantaneous value and the RMS value of the voltage at the wind power plant connection point are displayed. This variable has been selected because it shows the highest component percentage of the oscillation relative to the steady-state value.

In the recorded voltage, both the instantaneous and the RMS values show oscillations in two time windows: the first between 3 and 5 s and the second between 16 and 21 s, as highlighted in Figure 11. In this figure, it is important to emphasise that the change in the voltage reference causes the oscillation in the first time window, while in the second, the oscillation is caused by the sudden change in wind speed from 12.5 m/s to 9.5 m/s between 12 and 23 s. This confirms that in high-generation scenarios in weak networks, even without external disturbances, synchronous

17521424, 2026, 1, Downloaded from https://ietresearch.onlinelibrary.wiley.com/doi/10.1049/rpg2.70375 by Technical University Delft, Wiley Online Library on [15/10/2026]. See the Terms and Conditions (https://onlinelibrary.wiley.com/terms-and-conditions) on Wiley Online Library for rules of use; OA articles are governed by the applicable Creative Commons License

TABLE 4 | Sub-synchronous oscillation identified by using the RMS signals recorded during the change over time of wind speed.

	Prony		DMD		Wavelet	
Time window	**Freq. [Hz]**	**Damp. [%]**	**Freq. [Hz]**	**Damp. [%]**	**Freq. [Hz]**	**Damp. [%]**
16 s < t < 19 s	4.681	−6.346	4.488	−8.005	4.781	−6.129
19 s < t < 21 s	5.533	5.112	5.594	6.147	5.274	8.048

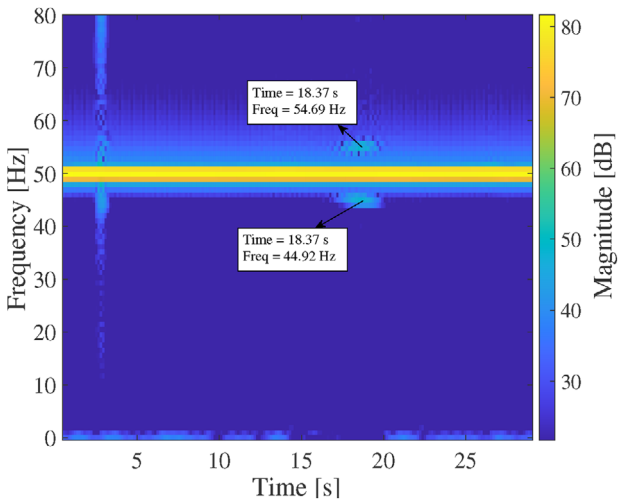


FIGURE 12 | STFT of instantaneous voltage of infinite bus system with a wind speed profile.

oscillations can occur due to the interaction between the controls and the system's equivalent impedance.

A first assessment of the oscillation is presented in Figure 12 through the spectrogram obtained from the performance of the STFT in the instantaneous voltage recorded from the simulation. In this figure, two frequencies are identified around the fundamental frequency in the time window from 16 to 21 s, corresponding to the sub-synchronous and super-synchronous components of the oscillations: 44.92 Hz and 54.69 Hz, respectively.

Finally, to characterise the oscillation, the time window from 16 to 21 s is divided into two intervals: from 16 to 19 s, when the oscillation amplitude increases, and from 19 to 21 s, when it decreases. Using prony and DMD, the frequency and damping of the two moments are presented in Table 4.

Based on the identified values, it is also possible to conclude that at 19 s, the oscillation decreases due to changes in wind speed. The frequency values across the two stages of the oscillation change slightly, highlighting the need to develop methods to identify non-stationary oscillations from measurements in converter-based systems, where multiple oscillatory modes with widely varying frequencies are present.

4.3 | Real-World Oscillation Events

Finally, to assess the methods under real operating conditions, data recorded during an event which leads to sub-synchronous oscillations is used. This event is part of a series of events reported by [99] (Australian Energy Market Operator) from August 2020 to December 2021 in the West Murray Zone (WMZ) of the interconnected networks in south-west New South Wales and north-west Victoria. The single line diagram of the West Murray Zone is presented in Figure 13. Although this event did not occur in an offshore power system, the system conditions, such as low inertia, low short-circuit ratio, and, above all, the high presence of converter-based generation, allow observation of operating conditions similar to those of offshore power systems.

The sub-synchronous oscillations observed in 2020 and 2021 had a frequency of 15-20 Hz and lasted from a few seconds to several minutes, occurring both with and without network disturbances. The principal causes of these oscillations are the low system strength in this area and the increasing penetration of converter-based generation.

In Figure 14, a recorded RMS voltage in phase 1 of a 220 kV bus, belonging to the WMZ area, is presented. In the recorded signal, the oscillation lasts about 1 min.

The first assessment to understand the main characteristics of the sub-synchronous oscillation is performed by applying the STFT to the recorded voltage measurements. The spectogram of the recorded RMS voltage is presented in Figure 15.

In this spectrogram, a sub-synchronous component is observed from 0.7 min and persists until 2 min, which is the duration of the recorded signal provided by AEMO. An important aspect to highlight in the spectrum is the change in the frequency value during the oscillation, starting from 17.87 Hz until 18.73 Hz, an increment of 0.86 Hz during the minute reported, which demonstrates the non-stationary nature of the oscillations, due, among other factors, to the variable nature of renewable generation sources and the low strength of the system.

Another insight from the spectrogram is that it registered only one oscillatory mode around 18 Hz; however, in the cases presented in the last two sections, the signals exhibit sub-synchronous and super-synchronous components. In the high-level report of the real-time observations [99], it is explained that the frequency obtained from the RMS signals corresponds to the aliased frequency in the phasor variables. Still, a deeper analysis of the instantaneous variables indicates that the signal has a principal component at 50 Hz ± 18 Hz (the identified frequency), resulting in a sub-synchronous component at 32 Hz and a super-synchronous component at 68 Hz.

In Table 5, the frequency and damping of the oscillatory mode presented in the recorded signals by AEMO are shown, using the

17521424, 2026, 1, Downloaded from https://ietresearch.onlinelibrary.wiley.com/doi/10.1049/rpg2.70375 by Technical University Delft, Wiley Online Library on [15/10/2026]. See the Terms and Conditions (https://onlinelibrary.wiley.com/terms-and-conditions) on Wiley Online Library for rules of use; OA articles are governed by the applicable Creative Commons License

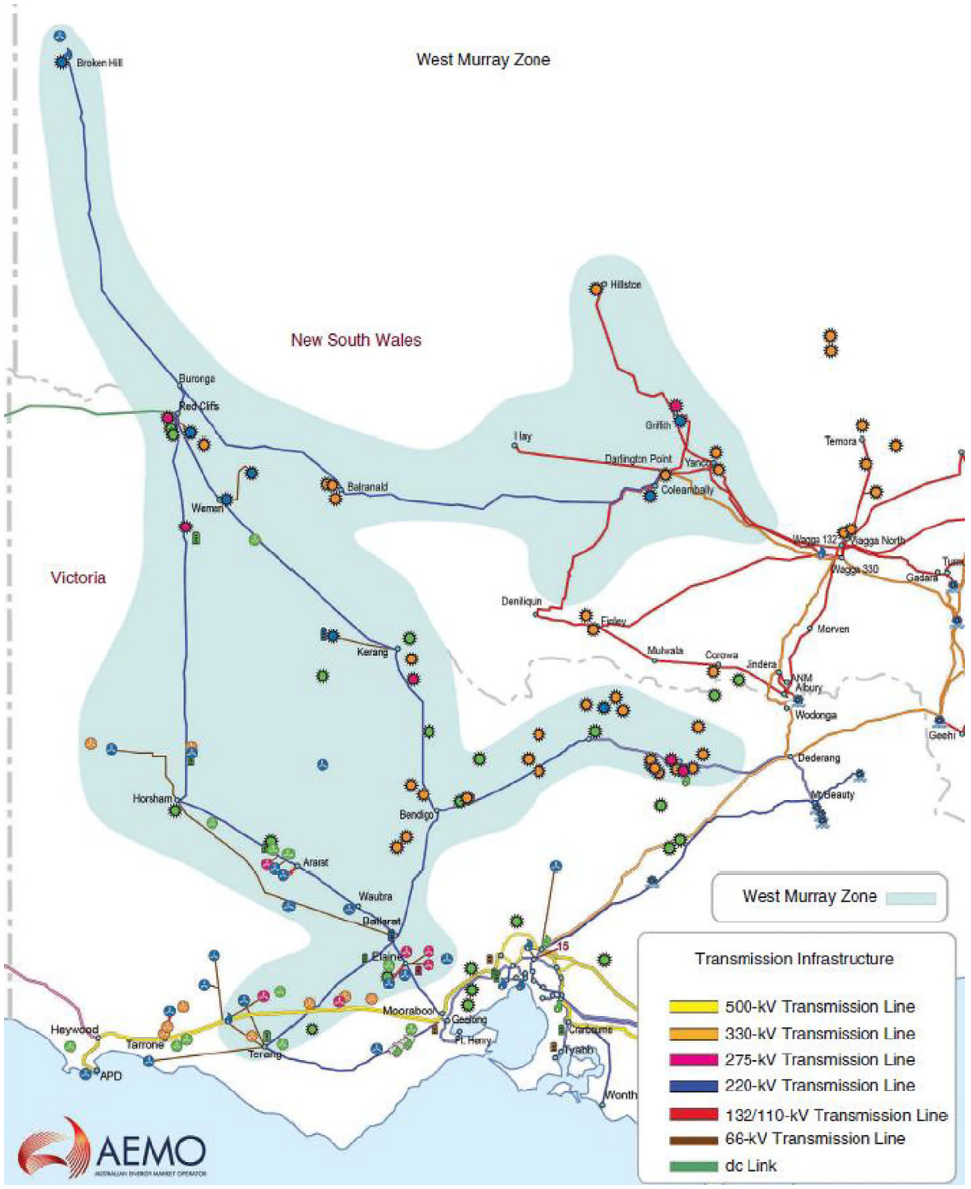


FIGURE 13 | West Murray Zone single line diagram. Source: reference [99].

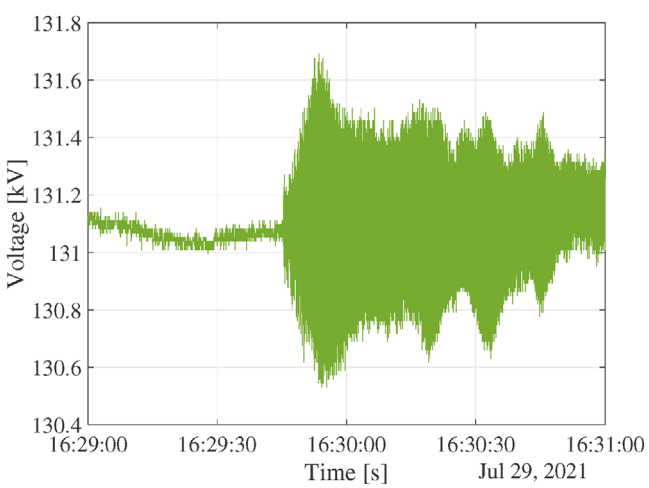


FIGURE 14 | Voltage measurements under sub-synchronous oscillation in the West Murray area. Source: AEMO.

TABLE 5 | Sub-synchronous oscillation parameters identified by using the RMS recorded signals.

	Prony		DMD	
Method	**Freq. [Hz]**	**Damp. [%]**	**Freq. [Hz]**	**Damp. [%]**
Value	18.273	0.601	18.273	0.921

prony and DMD method, with a time window of [0.7 s–2.0 s]. In this analysis, a mode of 18.27 Hz is obtained, with damping below 1% using both methods; however, as explained before, these methods cannot identify changes in the oscillation parameters, resulting in an identified stationary oscillation mode.

Finally, the wavelet continuous transformation is applied to this signal, and the magnitude scalogram is presented in Figure 16. In this figure, the changes in frequency and damping are shown,

17521424, 2026, 1, Downloaded from https://ietresearch.onlinelibrary.wiley.com/doi/10.1049/rpg2.70375 by Technical University Delft, Wiley Online Library on [15/10/2026]. See the Terms and Conditions (https://onlinelibrary.wiley.com/terms-and-conditions) on Wiley Online Library for rules of use; OA articles are governed by the applicable Creative Commons License

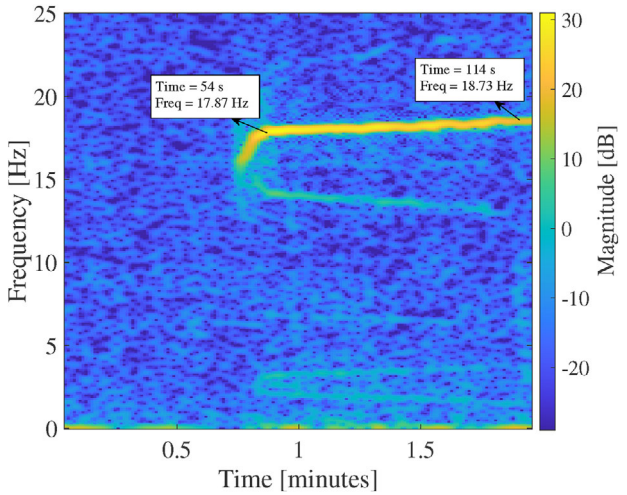


FIGURE 15 | Short-time frequency transform applied to a real-time data recorded by AEMO.

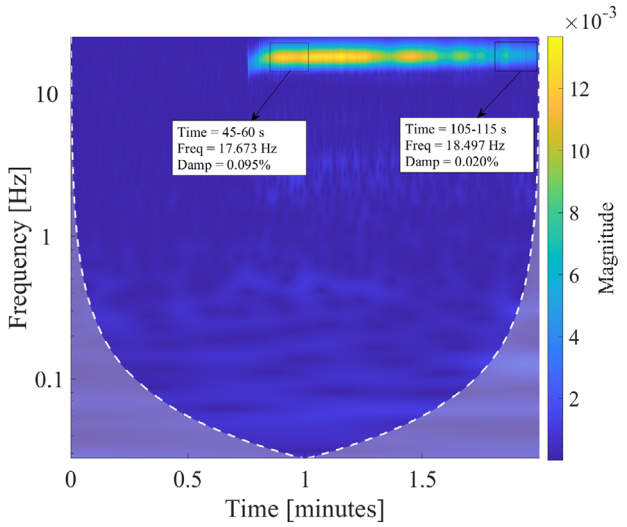


FIGURE 16 | Wavelet continuous transformation applied to RMS recorded signals.

with damping calculated over two time windows: the first is [45 s–60 s], with a damping of 0.095%, and the second is [105 s–115 s], with a damping of 0.02%. This result also demonstrates that both the frequency and the damping change over time. However, with the wavelet method, the choice of the time window depends on user experience, leading to an error percentage in the identified values. The mismatch between the damping obtained from the damping calculation with the time domain methods and the wavelet transform highlights the need for an enhanced method to calculate oscillation parameters in cases where the oscillations are non-stationary.

5 | Conclusions

This paper has presented a comprehensive review of sub-synchronous and SSO in modern power systems with high penetration of converter-based elements. An up-to-date classification of SSO was discussed, highlighting that, in converter-based environments, the dominant mechanisms are typically associated with interactions involving external capacitive components, weak grid conditions, and dynamic interactions among multiple control systems. The paper also reviewed the main oscillation identification methods currently available, emphasising the strengths and limitations of each approach. Importantly, these methods are applicable at different stages of power system planning and operation, and the selection of an appropriate method depends not only on identification accuracy but also on practical considerations, including the availability of system models, computational resources, and the specific objectives of the analysis.

The assessment of measurement-based identification methods revealed several challenges and opportunities for future research. FFT enables oscillation frequency identification with low computational overhead, making it well-suited for preliminary assessments; however, it does not provide information on damping or phase. The wavelet transform offers greater temporal resolution by revealing changes in oscillatory behaviour over time; however, to extract frequency and damping, it requires supplementary methods, thereby increasing computational load and making it more appropriate for supporting tasks such as time-window selection or trend analysis. Time-domain methods, by contrast, calculate both frequency and damping as stationary estimations and are generally the preferred choice for oscillation identification and control, assuming a stationary operating point. This stationarity requirement becomes a critical limitation in the context of SSO. Damping estimation becomes unreliable when signals are noisy or operating conditions vary, causing shifts in oscillation metrics that undermine identification and limit its utility for mitigation strategies. Also, because the damping in SSO is very small, sometimes close to zero, when the system is near an unstable operating point, small changes can make the relative error very large. Additionally, the system can exhibit multiple oscillations, and the methods can reasonably separate the frequencies, but the estimated amplitudes and decay rates can overlap, resulting in a poor response. The variability inherent to renewable generation is a primary driver of this difficulty, as it introduces non-stationary oscillatory behaviour that conventional techniques struggle to characterise. The presence of oscillatory modes across a wide frequency range, the rapid dynamic changes introduced by converter controls, and the influence of measurement noise increase the complexity in the identification task. Together, these factors underscore the need for advanced identification strategies that reliably capture SSO characteristics under realistic operating conditions.

The insights provided in this work can support the development of novel measurement-based methods that achieve more accurate and robust estimation of oscillation parameters, thereby enhancing the monitoring and secure operation of modern power systems.

Author Contributions

Camila Castrillón-Franco: conceptualisation, formal analysis, writing – original draft. **José Luis Rueda-Torres:** funding acquisition, project

17521424, 2026, 1, Downloaded from https://ietresearch.onlinelibrary.wiley.com/doi/10.1049/rpg2.70375 by Technical University Delft, Wiley Online Library on [15/10/2026]. See the Terms and Conditions (https://onlinelibrary.wiley.com/terms-and-conditions) on Wiley Online Library for rules of use; OA articles are governed by the applicable Creative Commons License

administration, supervision, writing – review & editing. **Arturo Román-Messina:** methodology, supervision, writing – review & editing.

Funding

The research work shown in this paper has received funding from TenneT TSO B.V within the research project on "Adaptive identification and mitigation of variable oscillatory phenomena in weakening networks - FORBES." It reflects only the authors views, and the aforesaid organization is not responsible for any use that may be made of the papers content.

Conflicts of Interest

The authors declare no conflicts of interest.

Data Availability Statement

Research data are not shared.

References

1. CIGRE JWG C4/B4.52, "Guidelines for Subsynchronous Oscillation Studies in Power Electronics Dominated Power Systems," Technical Brochure 909 (CIGRE, 2023).

2. IEEE PES Resource Center, "Wind Energy Systems Sub-Synchronous Oscillations: Events and Modeling" (IEEE, 2020).

3. D. Walker, C. Bowler, R. Jackson, and D. Hodges, "Results of Subsynchronous Resonance Test at Mohave," *IEEE Transactions on Power Apparatus and Systems* 94, no. 5 (1975): 1878–1889, https://doi.org/10.1109/T-PAS.1975.32034.

4. IEEE-SSR-Committee, "Readers Guide to Subsynchronous Resonance," *Transactions on Power Systems* 7, no. 1 (1992): 150–157.

5. R. Farmer, A. Schwalb, and E. Katz, "Navajo Project Report on Subsynchronous Resonance Analysis and Solutions," *IEEE Transactions on Power Apparatus and Systems* 96, no. 4 (1977): 1226–1232, https://doi.org/10.1109/T-PAS.1977.32445.

6. H. Khalilinia and J. Ghaisari, "Sub-Synchronous Resonance Damping in Series Compensated Transmission Lines Using a Statcom in the Common Bus," in *2009 IEEE Power and Energy Society General Meeting* (IEEE, 2009), 1–7.

7. K. Padiyar, *Analysis of Subsynchronous Resonance in Power Systems* (Springer, 1999).

8. X.-P. Zhang, Y. Li, C. Wu, J. Luo, and R. Zhang, "Sub-Synchronous Oscillation Phenomena Associated With Type-4 Wind Turbine Generators: A Review," *CSEE Journal of Power and Energy Systems* 11, no. 6 (2025): 2743–2762, https://doi.org/10.17775/CSEEJPES.2025.02220.

9. R. N. Damas, Y. Son, M. Yoon, S. Y. Kim, and S. Choi, "Subsynchronous Oscillation and Advanced Analysis: A Review," *IEEE Access* 8 (2020): 224020–224032, https://doi.org/10.1109/ACCESS.2020.3044634.

10. L. Fan, Z. Miao, S. Shah, et al., "Real-World 20-Hz IBR Subsynchronous Oscillations: Signatures and Mechanism Analysis," *IEEE Transactions on Energy Conversion* 37 (2022): 2863–2873, https://doi.org/10.1109/TEC.2022.3206795.

11. L. Yue and M. Hang, "Studies of Sub-Synchronous Oscillations in Large-Scale Wind Farm Integrated System," *IOP Conference Series: Earth and Environmental Science* 108, no. 5 (jan 2018): 052075, https://doi.org/10.1088/1755-1315/108/5/052075.

12. G. D. Irwin, A. K. Jindal, and A. L. Isaacs, "Sub-Synchronous Control Interactions Between Type 3 Wind Turbines and Series Compensated AC Transmission Systems," in *2011 IEEE Power and Energy Society General Meeting* (IEEE, 2011), 1–6.

13. X. Xie, X. Zhang, H. Liu, H. Liu, Y. Li, and C. Zhang, "Characteristic Analysis of Subsynchronous Resonance in Practical Wind Farms Connected to Series-Compensated Transmissions," *IEEE Transactions on Energy Conversion* 32, no. 3 (2017): 1117–1126, https://doi.org/10.1109/TEC.2017.2676024.

14. H. Liu, X. Xie, J. He, et al., "Subsynchronous Interaction Between Direct-Drive PMSG Based Wind Farms and Weak AC Networks," *IEEE Transactions on Power Systems* 32, no. 6 (2017): 4708–4720, https://doi.org/10.1109/TPWRS.2017.2682197.

15. C. Li, "Unstable Operation of Photovoltaic Inverter From Field Experiences," *IEEE Transactions on Power Delivery* 33, no. 2 (2018): 1013–1015, https://doi.org/10.1109/TPWRD.2017.2656020.

16. Department for Business, Energy & Industrial Strategy, "GB Power System Disruption on 9 August 2019—Energy Emergencies Executive Committee (E3C): Final Report" (2020).

17. N. Hatziargyriou, J. Milanovic, C. Rahmann, et al., "Definition and Classification of Power System Stability – Revisited and Extended," *IEEE Transactions on Power Systems* 36, no. 4 (2021): 3271–3281, https://doi.org/10.1109/TPWRS.2020.3041774.

18. IEEE, "Terms, Definitions and Symbols for Subsynchronous Oscillations," *IEEE Transactions on Power Apparatus and Systems* PAS-104, no. 6 (1985): 1326–1334, https://doi.org/10.1109/TPAS.1985.319152.

19. J. W. Ballance and S. Goldberg, "Subsynchronous Resonance in Series Compensated Transmission Lines," *IEEE Transactions on Power Apparatus and Systems* PAS-92, no. 5 (1973): 1649–1658, https://doi.org/10.1109/TPAS.1973.293713.

20. R. Bansal, "Three-Phase Self-Excited Induction Generators: An Overview," *IEEE Transactions on Energy Conversion* 20, no. 2 (2005): 292–299, https://doi.org/10.1109/TEC.2004.842395.

21. G. Singh, "Self-Excited Induction Generator Research—A Survey," *Electric Power Systems Research* 69, no. 2 (2004): 107–114, https://doi.org/10.1016/j.epsr.2003.08.004.

22. IEEE, "Reader's Guide to Subsynchronous Resonance," *IEEE Transactions on Power Systems* 7, no. 1 (1992): 150–157, https://doi.org/10.1109/59.141698.

23. V. Virulkar and G. Gotmare, "Sub-Synchronous Resonance in Series Compensated Wind Farm: A Review," *Renewable and Sustainable Energy Reviews* 55 (2016): 1010–1029, https://doi.org/10.1016/j.rser.2015.11.012.

24. K. Clark, "Overview of Subsynchronous Resonance Related Phenomena," in *PES T and D 2012* (IEEE, 2012), 1–3.

25. I. M. Canay, "A Novel Approach to the Torsional Interaction and Electrical Damping of the Synchronous Machine Part I: Theory," *IEEE Transactions on Power Apparatus and Systems* PAS-101, no. 10 (1982): 3630–3638, https://doi.org/10.1109/TPAS.1982.317048.

26. M. Bahrman, E. Larsen, R. Piwko, and H. Patel, "Experience with HVDC - Turbine-Generator Torsional Interaction at Square Butte," *IEEE Transactions on Power Apparatus and Systems* PAS-99, no. 3 (1980): 966–975, https://doi.org/10.1109/TPAS.1980.319726.

27. C. Zhou and Z. Xu, "Damping Analysis of Subsynchronous Oscillation Caused by HVDC," in *2003 IEEE PES Transmission and Distribution Conference and Exposition (IEEE Cat. No.03CH37495)*, Vol. 1 (IEEE, 2003), 30–34.

28. N. Rostamkolai, R. Piwko, E. Larsen, D. Fisher, M. Mobarak, and A. Poitras, "Subsynchronous Interactions With Static VAR Compensators-Concepts and Practical Implications," *IEEE Transactions on Power Systems* 5, no. 4 (1990): 1324–1332, https://doi.org/10.1109/59.99384.

29. N. Rostamkolai, R. Piwko, E. Larsen, D. Fisher, M. Mobarak, and A. Poltras, "Subsynchronous Torsional Interactions With Static VAR Compensators-Influence of HVDC," *IEEE Transactions on Power Systems* 6, no. 1 (1991): 255–261, https://doi.org/10.1109/59.131070.

30. R. K. Varma, S. Auddy, and Y. Semsedini, "Mitigation of Subsynchronous Resonance in a Series-Compensated Wind Farm Using FACTS Controllers," *IEEE Transactions on Power Delivery* 23, no. 3 (2008): 1645–1654, https://doi.org/10.1109/TPWRD.2008.917699.

17521424, 2026, 1, Downloaded from https://ietresearch.onlinelibrary.wiley.com/doi/10.1049/rpg2.70375 by Technical University Delft, Wiley Online Library on [15/10/2026]. See the Terms and Conditions (https://onlinelibrary.wiley.com/terms-and-conditions) on Wiley Online Library for rules of use; OA articles are governed by the applicable Creative Commons License

31. J. Shair, X. Xie, L. Wang, W. Liu, J. He, and H. Liu, "Overview of Emerging Subsynchronous Oscillations in Practical Wind Power Systems," *Renewable and Sustainable Energy Reviews* 99 (2019): 159–168, https://doi.org/10.1016/j.rser.2018.09.047.

32. S. Jayaram Kumar, A. Ghosh, and Sachchidanand, "Damping of Subsynchronous Resonance Oscillations With TCSC and PSS and Their Control Interaction," *Electric Power Systems Research* 54, no. 1 (2000): 29–36, https://doi.org/10.1016/S0378-7796(99)00070-X.

33. X. Liu, Z. Xu, and Z. Zhang, "Influence of PSS on Subsynchronous Oscillation Characteristics in LCC-HVDC System and the Corresponding Restraint Measures," in *2020 4th International Conference on HVDC (HVDC)* (IEEE, 2020), 692–697.

34. J. Lyu, X. Cai, M. Amin, and M. Molinas, "Sub-Synchronous Oscillation Mechanism and Its Suppression in MMC-Based HVDC Connected Wind Farms," *IET Generation, Transmission & Distribution* 12, no. 4 (2018): 1021–1029, https://doi.org/10.1049/iet-gtd.2017.1066.

35. B. Shao, S. Zhao, Y. Yang, B. Gao, and F. Blaabjerg, "Sub-Synchronous Oscillation Characteristics and Analysis of Direct-Drive Wind Farms With VSC-HVDC Systems," *IEEE Transactions on Sustainable Energy* 12, no. 2 (2021): 1127–1140, https://doi.org/10.1109/TSTE.2020.3035203.

36. C. Yin, X. Xie, S. Xu, and C. Zou, "Review of Oscillations in VSC-HVDC Systems Caused by Control Interactions," *The Journal of Engineering* 2019, no. 16 (2019): 1204–1207.

37. Y. Cheng, L. Fan, J. Rose, et al., "Real-World Subsynchronous Oscillation Events in Power Grids With High Penetrations of Inverter-Based Resources," *IEEE Transactions on Power Systems* 38, no. 1 (2023): 316–330, https://doi.org/10.1109/TPWRS.2022.3161418.

38. Y. Xu, S. Zhao, Y. Cao, and K. Sun, "Understanding Subsynchronous Oscillations in DFIG-Based Wind Farms Without Series Compensation," *IEEE Access* 7 (2019): 107201–107210.

39. S. Kovacevic, D. Jovcic, S. S. Aphale, P. Rault, and O. Despouys, "Analysis of Potential Low Frequency Resonance Between a 1GW MMC HVDC and a Nearby Nuclear Generator," *Electric Power Systems Research* 187 (2020): 106491, https://doi.org/10.1016/j.epsr.2020.106491.

40. C. Karawita, "HVDC Interaction Studies Using Small Signal Stability Assessment" (University of Manitoba, 2019).

41. P. Kundur, *Power System Stability and Control* (McGraw-Hill Education, 1993).

42. F. Kelada, J. Buire, and N. Hadjsaid, "Revisiting Small-Signal Modeling for Analyzing Fast Dynamic Interactions in Converter-Dominated Power Systems," *IEEE Transactions on Power Systems* 40 (2025): 3819–3832, https://doi.org/10.1109/TPWRS.2025.3550287.

43. A. Kuri, R. Zurowski, G. Mehlmann, and M. Luther, "Converter Modelling Aspects at the Boundary Between EMT and RMS Domain," in *2022 International Conference on Smart Energy Systems and Technologies (SEST)* (IEEE, 2022), 1–6.

44. J. Arevalo-Soler, D. Moutevelis, E. Mateu-Barriendos, et al., "A Matlab-based Toolbox for Automatic EMT Modeling and Small-Signal Stability Analysis of Modern Power Systems," arxiv:2506.22201 (2025).

45. J. Sun, "Impedance-Based Stability Criterion for Grid-Connected Inverters," *IEEE Transactions on Power Electronics* 26 (2011): 3075–3078, https://doi.org/10.1109/TPEL.2011.2136439.

46. H. Liu, X. Xie, and W. Liu, "An Oscillatory Stability Criterion Based on the Unified dq-Frame Impedance Network Model for Power Systems With High-Penetration Renewables," *IEEE Transactions on Power Systems* 33 (2018): 3472–3485, https://doi.org/10.1109/TPWRS.2018.2794067.

47. M. Sahni, D. Muthumuni, B. Badrzadeh, A. Gole, and A. Kulkarni, "Advanced Screening Techniques for Sub- Synchronous Interaction in Wind Farms," in *PES T and D 2012* (IEEE, 2012).

48. B. Badrzadeh, M. Sahni, Y. Zhou, D. Muthumuni, and A. Gole, "General Methodology for Analysis of Sub-Synchronous Interaction," *IEEE Transactions on Power Systems* 28 (2013): 1858–1869, https://doi.org/10.1109/TPWRS.2012.2225850.

49. F. Shi, D. Shu, Z. Yan, and Z. Song, "A Shifted Frequency Impedance Model of Doubly Fed Induction Generator (DFIG)-Based Wind Farms and Its Applications on S^2SI Analysis," *IEEE Transactions on Power Electronics* 36 (2021): 215–227, https://doi.org/10.1109/TPEL.2020.2999113.

50. L. Fan and Z. Miao, "Admittance-Based Stability Analysis: Bode Plots, Nyquist Diagrams or Eigenvalue Analysis?," *IEEE Transactions on Power Systems* 35 (2020): 3312–3315, https://doi.org/10.1109/TPWRS.2020.2996014.

51. X. Wang, F. Blaabjerg, and W. Wu, "Modeling and Analysis of Harmonic Stability in an AC Power-Electronics-Based Power System," *IEEE Transactions on Power Electronics* 29 (2014): 6421–6432, https://doi.org/10.1109/TPEL.2014.2306432.

52. C. Zhang, M. Molinas, A. Rygg, and X. Cai, "Impedance-Based Analysis of Interconnected Power Electronics Systems: Impedance Network Modeling and Comparative Studies of Stability Criteria," *IEEE Journal of Emerging and Selected Topics in Power Electronics* 8 (2020): 2520–2533, https://doi.org/10.1109/JESTPE.2019.2914560.

53. L. Fan and Z. Miao, "Nyquist Stability Criterion Based SSR Explanation for Type 3 Wind Generators," *IEEE Transactions on Energy Conversion* 27, no. 3 (2012): 807–809.

54. H. Nyquist, "Certain Topics in Telegraph Transmission Theory," *Transactions of the American Institute of Electrical Engineers* 47, no. 2 (1928): 617–644, https://doi.org/10.1109/T-AIEE.1928.5055024.

55. C. E. Shannon, "A Mathematical Theory of Communication," *Bell System Technical Journal* 27, no. 3 (1948): 379–423, https://doi.org/10.1002/j.1538-7305.1948.tb01338.x.

56. O. D. Fernández, S. Tiistola, and A. Gusrialdi, "Real-Time Data-Driven Electromechanical Oscillation Monitoring using Dynamic Mode Decomposition with Sliding Window," *IFAC-PapersOnLine* 55, no. 9 (2022): 158–163, https://doi.org/10.1016/j.ifacol.2022.07.028.

57. A. Liccardo, S. Tessitore, F. Bonavolontà, et al., "Detection and Analysis of Inter-Area Oscillations Through a Dynamic-Order DMD Approach," *IEEE Transactions on Instrumentation and Measurement* 71 (2022): 1–14, https://doi.org/10.1109/TIM.2022.3186371.

58. M. H. Bollen, I. Y. Gu, S. Santoso, et al., "Bridging the Gap Between Signal and Power: Assessing Power System Quality Using Signal Processing Techniques," *IEEE Signal Processing Magazine* 26 (2009): 12–31, https://doi.org/10.1109/MSP.2009.932706.

59. L. Vanfretti, L. Dosiek, J. W. Pierre, et al., "Application of Ambient Analysis Techniques for the Estimation of Electromechanical Oscillations From Measured PMU Data in Four Different Power Systems," *European Transactions on Electrical Power* 21, no. 4 (2011): 1640–1656, https://doi.org/10.1002/etep.507.

60. K. G. Ranjan, B. R. Prusty, and D. Jena, "Review of Preprocessing Methods for Univariate Volatile Time-Series in Power System Applications," *Electric Power Systems Research* 191 (2021): 106885.

61. M. Netto and L. Mili, "A Robust Prony Method for Power System Electromechanical Modes Identification," in *IEEE Power & Energy Society General Meeting* (IEEE, 2017).

62. J. Shair, X. Xie, and G. Yan, "Mitigating Subsynchronous Control Interaction in Wind Power Systems: Existing Techniques and Open Challenges," *Renewable and Sustainable Energy Reviews* 108 (2019): 330–346.

63. A. Almunif, L. Fan, and Z. Miao, "A Tutorial on Data-Driven Eigenvalue Identification: Prony Analysis, Matrix Pencil, and Eigensystem Realization Algorithm," *International Transactions on Electrical Energy Systems* 30 (2020): e12283.

64. A. J. Allen, M. Singh, E. Muljadi, and S. Santoso, "Measurement-Based Investigation of Inter- and Intra-Area Effects of Wind Power Plant Integration," *International Journal of Electrical Power and Energy Systems* 83 (2016): 450–457, https://doi.org/10.1016/j.ijepes.2016.04.025.

65. Y. Zhao and Y. Liu, "Wide-Band Oscillation Detection Using High-Speed Synchrophasor Measurements Based on a Time-Frequency

17521424, 2026, 1, Downloaded from https://ietresearch.onlinelibrary.wiley.com/doi/10.1049/rpg2.70375 by Technical University Delft, Wiley Online Library on [15/10/2026]. See the Terms and Conditions (https://onlinelibrary.wiley.com/terms-and-conditions) on Wiley Online Library for rules of use; OA articles are governed by the applicable Creative Commons License

Method," in *2024 IEEE Power And Energy Society General Meeting (PESGM)* (IEEE, 2024), 1–5.

66. M. Wang and Y. Sun, "A Practical Method to Improve Phasor and Power Measurement Accuracy of DFT Algorithm," *IEEE Transactions on Power Delivery* 21, no. 3 (2006): 1054–1062, https://doi.org/10.1109/TPWRD.2005.858769.

67. D. Cai, Y. Ma, Z. Zhang, Q. Huang, and J. Li, "Estimation of Subsynchronous Oscillation Using a Sliding Window Iterative DFT Algorithm," in *2021 3rd Asia Energy and Electrical Engineering Symposium (AEEES)* (IEEE, 2021), 337–340.

68. S. Xiuping, L. Qian, J. Shijie, and X. Yong, "The Analysis System of Online Monitoring and Disturbance Source Locating for Subsynchronous Oscillation Based on D5000 Platform," in *IEEE 2nd International Conference on Electronics Technology (ICET)* (IEEE, 2019), 515–519.

69. T. Hiyama, N. Suzuki, and T. Funakoshi, "On-Line Identification of Power System Oscillation Modes by Using Real Time FFT," in *2000 IEEE Power Engineering Society Winter Meeting. Conference Proceedings (Cat. No.00CH37077)*, Vol. 2 (IEEE, 2000), 1521–1526.

70. A. Alkan and A. S. Yilmaz, "Frequency Domain Analysis of Power System Transients Using Welch and Yule–Walker AR Methods," *Energy Conversion and Management* 48, no. 7 (2007): 2129–2135, https://doi.org/10.1016/j.enconman.2006.12.017.

71. S.-F. Chou, X. Wang, and F. Blaabjerg, "Frequency-Domain Modal Analysis for Power-Electronic-Based Power Systems," *IEEE Transactions on Power Electronics* 36, no. 5 (2021): 4910–4914, https://doi.org/10.1109/TPEL.2020.3032736.

72. Y. Mitani and L. Qing, "Application of HHT for Oscillation Mode Analysis in Power System Based on PMU," in *International Conference on Electric Power and Energy Conversion Systems (EPECS)* (IEEE, 2011).

73. J. G. Philip, J. Jung, and A. Onen, "Empirical Wavelet Transform Based Method for Identification and Analysis of Sub-synchronous Oscillation Modes Using PMU Data," *Journal of Modern Power Systems and Clean Energy* 12, no. 1 (2024): 34–40, https://doi.org/10.35833/MPCE.2023.000047.

74. T. Ji, S. Wang, L. Zhang, and Q. H. Wu, "Sub/Super-Synchronous Oscillation Detection Based on Matching Synchroextracting Wavelet Transform," *CSEE Journal of Power and Energy Systems* 11, no. 2 (2025): 649–660, https://doi.org/10.17775/CSEEJPES.2023.01310.

75. A. Roman-Messina, E. R. Murillo-Aguirre, M. A. Hernandez-Ortega, and C. A. Morales-Regis, "Time-Frequency Characterization of Dynamic Phase Synchrony in Power Grids," *IEEE Access* 13 (2025): 184147–184158, https://doi.org/10.1109/ACCESS.2025.3625398.

76. Q. Lin, Y.-F. Zhang, F. Xue, and G. Yu, "Parameter Identification Method for Sub-Synchronous Oscillation Signals in Power Systems Based on Improved Multi-Synchrosqueezing Transform and Automatic Recognition Algorithm," *Neural Computing and Applications* 37, no. 5 (2025): 3719–3732.

77. D. Li, J. Yang, C. Tian, et al., "Parameter Identification of Sub-Synchronous Oscillation in New Power Systems Based on the Improved VMD-Prony Algorithm," in *International Conference on Mechanical, Electronics and Electrical and Automation Control (METMS)* (IEEE, 2025), 75–82.

78. H. Yu, Z. Zhang, S. Li, H. Wang, J. Bian, and G. Li, "Dynamic Monitoring and Identification Method for Sub-Synchronous Oscillation in Wind Power Grid-Integrated Systems Under a Three-Level Collaborative Architecture," *International Journal of Electrical Power and Energy Systems* 175 (2026): 111651, https://doi.org/10.1016/j.ijepes.2026.111651.

79. H. Liu, Y. Qi, J. Zhao, and T. Bi, "Data-Driven Subsynchronous Oscillation Identification Using Field Synchrophasor Measurements," *IEEE Transactions on Power Delivery* 37 (2022): 165–175, https://doi.org/10.1109/TPWRD.2021.3054889.

80. Y. Wang, H. Yang, X. Xie, X. Yang, and G. Chen, "Real-time Subsynchronous Control Interaction Monitoring Using Improved Intrinsic Time-scale Decomposition," *Journal of Modern Power Systems and Clean Energy* 11 (2023): 816–826, https://doi.org/10.35833/MPCE.2021.000464.

81. B. Ren, Q. Li, Y. Jia, Q. Zhou, C. Wang, and X. Zou, "A Machine Learning Method for Locating Subsynchronous Oscillation Source of VSCs in Wind Farm Induced by Open-Loop Modal Resonance Based on Measurement," *Frontiers in Energy Research* 10 (2023): 1047624, https://doi.org/10.3389/fenrg.2022.1047624.

82. L. Li, Y. Mao, Z. Liang, et al., "Subsynchronous Oscillation Analysis Method Based on Broad Learning System," *Energy Reports* 9 (2023): 221–234, https://doi.org/10.1016/j.egyr.2023.04.066.

83. G. Liu, J. Liu, and A. Liu, "Sub-Synchronous Oscillation Suppression Strategy in Wind Power Systems With DFIGs Based on Improved Deep Reinforcement Learning Algorithms," *Electric Power Systems Research* 248 (2025): 111959, https://doi.org/10.1016/j.epsr.2025.111959.

84. H. Mohsenian-Rad and W. Xu, "Synchro-Waveforms: A Window to the Future of Power Systems Data Analytics," *IEEE Power and Energy Magazine* 21 (2023): 68–77, https://doi.org/10.1109/MPE.2023.3288583.

85. M. Izadi and H. Mohsenian-Rad, "A Synchronized Lissajous-Based Method to Detect and Classify Events in Synchro-Waveform Measurements in Power Distribution Networks," *IEEE Transactions on Smart Grid* 13 (2022): 2170–2184, https://doi.org/10.1109/TSG.2022.3148757.

86. K.-P. Poon and K.-C. Lee, "Analysis of Transient Stability Swings in Large Interconnected Power Systems by Fourier Transformation," *IEEE Transactions on Power Systems* 3, no. 4 (1988): 1573–1581.

87. J. B. Allen and L. R. Rabiner, "A Unified Approach to Short-Time Fourier Analysis and Synthesis," *Proceedings of the IEEE* 65, no. 11 (1977): 1558–1564, https://doi.org/10.1109/PROC.1977.10770.

88. J. G. Proakis and D. G. Manolakis, *Digital Signal Processing: Principles, Algorithms, and Applications* (Pearson, 2006).

89. J. F. Hauer, C. Demeure, and L. L. Scharf, "Initial Results in Prony Analysis of Power System Response Signals," *IEEE Transactions on Power Systems* 5, no. 1 (2002): 80–89.

90. J. H. Tu, C. W. Rowley, D. M. Luchtenburg, S. L. Brunton, and J. N. Kutz, "On Dynamic Mode Decomposition: Theory and Applications," *Journal of Computational Dynamics* 1, no. 2 (2013): 391–421, https://doi.org/10.3934/jcd.2014.1.391.

91. P. J. Schmid, L. Li, M. P. Juniper, and O. Pust, "Applications of the Dynamic Mode Decomposition," *Theoretical and Computational Fluid Dynamics* 25 (2011): 249–259, https://doi.org/10.1007/s00162-010-0203-9.

92. E. Barocio, B. C. Pal, N. F. Thornhill, and A. R. Messina, "A Dynamic Mode Decomposition Framework for Global Power System Oscillation Analysis," *IEEE Transactions on Power Systems* 30 (2015): 2902–2912, https://doi.org/10.1109/TPWRS.2014.2368078.

93. S. Mallat, *A Wavelet Tour of Signal Processing* (Academic Press, 1999).

94. J. L. Rueda, C. A. Juárez, and I. Erlich, "Wavelet-Based Analysis of Power System Low-Frequency Electromechanical Oscillations," *IEEE Transactions on Power Systems* 26 (2011): 1733–1743, https://doi.org/10.1109/TPWRS.2010.2104164.

95. S. Wang, J. Zhao, Z. Huang, and R. Diao, "Assessing Gaussian Assumption of PMU Measurement Error Using Field Data," *IEEE Transactions on Power Delivery* 33 (2018): 3233–3236, https://doi.org/10.1109/TPWRD.2017.2762927.

96. *Standardization of Renewable Energy System Modelling Example Case* (RTDS, 2022).

97. N. Pahalawaththa and S. Achilles, "Connection of Wind Farms to Weak AC Networks," Working Group WG B4.62 (CIGRE, 2016).

98. J. Marchand, "EMT Model and Dynamic Power Management Strategy of an Offshore Renewable Energy Hub With Local Power-to-Gas Conversion" (2021).

99. *West Murray Zone Sub-Synchronous Oscillations* (AEMO, 2022).

17521424, 2026, 1, Downloaded from https://ietresearch.onlinelibrary.wiley.com/doi/10.1049/rpg2.70375 by Technical University Delft, Wiley Online Library on [15/10/2026]. See the Terms and Conditions (https://onlinelibrary.wiley.com/terms-and-conditions) on Wiley Online Library for rules of use; OA articles are governed by the applicable Creative Commons License